Journal of Fluid Mechanics
http://journals.cambridge.org/FLM

Additional services for ***Journal of Fluid Mechanics:***

Email alerts: Click here
Subscriptions: Click here
Commercial reprints: Click here
Terms of use : Click here

Heat release rate correlation and combustion noise in premixed flames

N. SWAMINATHAN, G. XU, A. P. DOWLING and R. BALACHANDRAN

Journal of Fluid Mechanics / Volume 681 / August 2011, pp 80 - 115
DOI: 10.1017/jfm.2011.232, Published online: 29 June 2011

Link to this article: http://journals.cambridge.org/abstract_S0022112011002321

How to cite this article:
N. SWAMINATHAN, G. XU, A. P. DOWLING and R. BALACHANDRAN (2011). Heat release rate correlation and combustion noise in premixed flames. Journal of Fluid Mechanics, 681, pp 80-115 doi:10.1017/jfm.2011.232

Request Permissions : Click here

CAMBRIDGE JOURNALS

Downloaded from http://journals.cambridge.org/FLM, IP address: 144.82.107.38 on 02 Nov 2012

J. Fluid Mech. (2011), *vol.* 681, *pp.* 80–115. © Cambridge University Press 2011
doi:10.1017/jfm.2011.232

Heat release rate correlation and combustion noise in premixed flames

N. SWAMINATHAN[1]†, G. XU[1]‡, A. P. DOWLING[1] AND R. BALACHANDRAN[2]

[1]Department of Engineering, Cambridge University, Cambridge CB2 1PZ, UK

[2]Department of Mechanical Engineering, University College London, London WC1E 7JE, UK

(Received 11 March 2010; revised 14 April 2011; accepted 16 May 2011; first published online 29 June 2011)

The sound emission from open turbulent flames is dictated by the two-point spatial correlation of the rate of change of the fluctuating heat release rate. This correlation in premixed flames can be represented well using Gaussian-type functions and unstrained laminar flame thermal thickness can be used to scale the correlation length scale, which is about a quarter of the planar laminar flame thermal thickness. This correlation and its length scale are observed to be less influenced by the fuel type or stoichiometry or turbulence Reynolds and Damkohler numbers. The time scale for fluctuating heat release rate is deduced to be about $\tau_c/34$ on an average, where τ_c is the planar laminar flame time scale, using direct numerical simulation (DNS) data. These results and the spatial distribution of mean reaction rate obtained from Reynolds-averaged Navier–Stokes (RANS) calculations of open turbulent premixed flames employing the standard $\widetilde{k}$–$\widetilde{\varepsilon}$ model and an algebraic reaction rate closure, involving a recently developed scalar dissipation rate model, are used to obtain the far-field sound pressure level from open flames. The calculated values agree well with measured values for flames of different stoichiometry and fuel types, having a range of turbulence intensities and heat output. Detailed analyses of RANS results clearly suggest that the noise level from turbulent premixed flames having an extensive and uniform spatial distribution of heat release rate is low.

Key words: acoustics, reacting flows, turbulent reacting flows

1. Introduction

Lean burning has been identified as the potential way forward to reduce pollutants emission from engines used for air and surface transports. However, this mode of burning is known to be unstable involving highly unsteady flames, which emit acoustic waves. The noise coming from these waves is emerging as an important source of noise in lean-burn systems in general and specifically for gas turbines partly because other noise sources have been reduced. Hence, the combustion noise emitted by highly fluctuating flames needs to be addressed. A thorough understanding of these sources and their behaviours at a fundamental level is a necessary requirement to devise strategies to mitigate combustion noise from lean-burn systems.

† Email address for correspondence: ns341@cam.ac.uk

‡ On sabbatical leave from the Institute of Engineering Thermophysics, Chinese Academy of Sciences, Beijing 100080, China.

Many studies (Price, Hurle & Sugden 1968; Hurle *et al.* 1968; Strahle 1978; Jones 1979; Crighton *et al.* 1992, for example) in the past have tried to address the combustion noise problem and identified that the source mechanism for this noise is the fluctuating heat release rate. These fluctuations cause changes in the local dilatation, which act as monopole sources for sound generation. From a practical point of view, there are two primary mechanisms of sound generation in combustion systems. The first mechanism is directly related to the unsteady combustion process and the noise generated by this mechanism is known as *direct noise*. The second mechanism is due to the acceleration of convected hot spots, i.e. accelerating inhomogeneous density field and the noise due to this mechanism is known as *indirect noise*. As discussed in § 2, a model for the two-point correlation of the rate of change of the fluctuating heat release rate is central to predicting both direct and indirect noises. This two-point correlation has not been investigated sufficiently in the literature and a recent study (Swaminathan *et al.* 2011) suggested that the integral length scale for this correlation is nearly 60 times smaller than the typical values used in many earlier studies. Furthermore, this correlation length scale is observed (Swaminathan *et al.* 2011) to scale with planar laminar flame thermal thickness rather than with a turbulence length scale and thus it does not depend on the turbulence Reynolds number or swirl in the flow. There are four objectives of this study, namely (i) to provide the theoretical background for the two-point cross-correlation and its analysis briefly introduced in our preliminary investigation (Swaminathan *et al.* 2011); (ii) to investigate the cross-correlations of the fluctuating reaction rate and its rate of change in order to demonstrate their dependence on fuel type and its stoichiometry, and Damköhler number; (iii) to assess a model for the cross-correlation, which can be used in conjunction with RANS (Reynolds-averaged Navier–Stokes) calculation, by predicting far-field sound pressure level (SPL) from open turbulent premixed methane- and propane–air flames for a range of thermochemical and fluid dynamic conditions, and heat load; and (iv) to demonstrate the linearity between the root-mean-square (r.m.s.) value of the fluctuating reaction rate and mean reaction rate. As noted in § 2.2, this linear relation is required to close the problem of predicting the far-field SPL using the RANS approach. The RANS results are analysed further to develop an understanding of the relationship between the far-field SPL and the spatial distribution of the mean heat release rate inside flame brush.

Let us consider an example of an open turbulent premixed flame as shown in figure 1. The far-field sound pressure fluctuation resulting from the direct noise is given by

$$p'(\boldsymbol{r}, t) = \frac{(\gamma - 1)}{4\pi r a_o^2} \frac{\partial}{\partial t} \int_{v_y} \dot{Q}\left(\boldsymbol{y},\, t - \frac{r}{a_o}\right) \mathrm{d}^3 y, \tag{1.1}$$

where the region v_y undergoing turbulent combustion or the *flame brush* is compact. The symbols t, $\boldsymbol{y}$ and $r = |\boldsymbol{r}|$, respectively, denote the time, the position inside the flame brush and the distance of the observer as noted in figure 1. The speed of sound at ambient conditions surrounding the combustion region is denoted by a_o and the instantaneous heat release rate per unit volume is $\dot{Q}$. A brief derivation of this equation starting from the Lighthill equation is presented in § 2, which also identifies other acoustic sources of secondary nature in turbulent reacting flows. Equation (1.1) clearly shows that the rate of change of heat release rate generates pressure fluctuation and this expression applies to turbulent premixed, non-premixed and partially premixed combustion modes. Also, note that the fine details of heat release mechanisms and their physics in these different combustion modes may influence the characteristics of

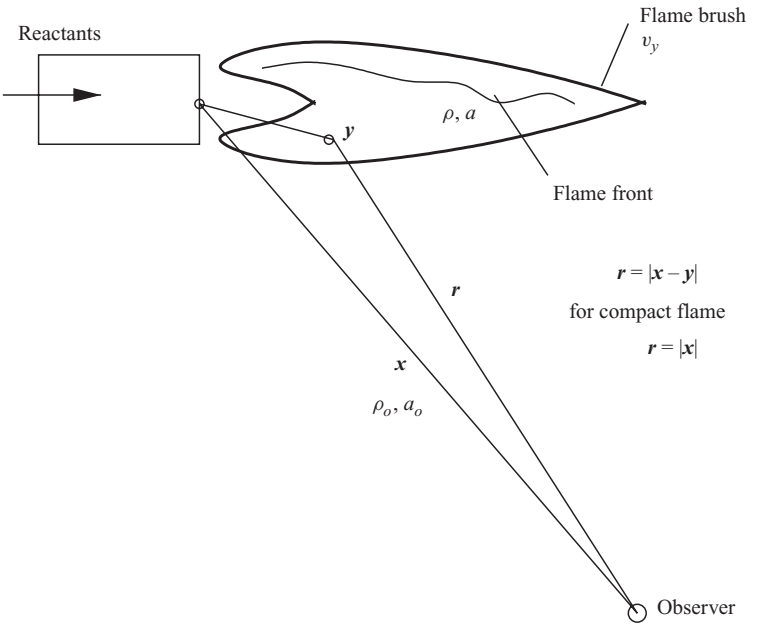

FIGURE 1. Schematic diagram showing the turbulent flame brush and coordinates for analysis.

p', but (1.1) clearly notes that the integral value drives the pressure fluctuation and thus the direct noise only depends on the combustion mode through its influence on the rate of change of the total rate of heat released, as noted by Price *et al.* (1968) and Strahle (1971). However, the following points can be noted from a number of studies on combustion noise emitted by premixed (Price *et al.* 1968; Strahle 1978; Strahle & Shivashankara 1975; Kilham & Kirmani 1979; Kotake & Takamoto 1987, 1990; Rajaram & Lieuwen 2003; Hirsch *et al.* 2007), non-premixed (Ohiwa, Tanaka & Yamaguchi 1993; Klein & Kok 1999; Singh, Frankel & Gore 2004; Flemming, Sadiki & Janicka 2007; Ihme, Pitsch & Bodony 2009) and partially premixed (Singh *et al.* 2005; Duchaine, Zimmer & Schuller 2009) flames: (i) the combustion noise has a broadband spectrum with a peak sound level of about 60–80 dB in the frequency range of about 200–1000 Hz, (ii) the overall SPL increases with the fuel flow rate and the heating value of the fuel, (iii) there is a considerable increase in the SPL if one mixes air with the fuel (Singh *et al.* 2005) so that the equivalence ratio stays beyond the rich flammability limit; however, this observed increase might be due to room resonance since the experiment was not carried out in an anechoic environment. Even in liquid–fuel spray combustion (Price *et al.* 1968), the acoustic source may be represented by a collection of monopoles as suggested by (1.1).

A review of combustion modelling studies will clearly identify that the spatial structure of heat release rate, $\dot{Q}(\boldsymbol{y}, t)$, strongly depends on the combustion mode, characteristics of the background turbulence and its interaction. Thus, the distribution of acoustic source will duly be influenced by these factors. Hence, it is inevitable to confine the combustion noise analysis to a particular combustion mode and we confine ourselves to open turbulent premixed flames. Future investigations will address other modes.

The combustion noise generated by open turbulent premixed flames has been investigated experimentally (Price *et al.* 1968; Hurle *et al.* 1968; Strahle &

Shivashankara 1975; Strahle 1978; Kilham & Kirmani 1979; Kotake & Takamoto 1987, 1990; Rajaram & Lieuwen 2003; Hirsch *et al.* 2007), theoretically (Bragg 1963; Strahle 1971; Kotake 1975; Strahle 1976; Clavin & Siggia 1991) and numerically (Hirsch *et al.* 2007) in the past. These studies have predominantly tried to develop a semi-empirical correlation for either far-field acoustic power or acoustic efficiency. These two quantities are defined in § 2. The semi-empirical correlations for the acoustic efficiency of high-Damköhler-number flames, defined in § 3, may be written in a generic form as $\eta_{ac} \sim \hat{Da}^{b_1} \hat{Re}^{b_2} Y_F^{b_3} Ma^{b_4} \hat{H}^{b_5}$, where $\hat{Da}$ is a Damköhler number involving a convective time scale defined using the bulk-mean velocity and burner diameter, $\hat{Re}$ is the Reynolds number based on burner diameter and bulk-mean velocity of reactant flow with fuel mass fraction Y_F, Ma is the Mach number and $\hat{H}$ is an appropriately normalised lower heating value of the fuel. The exponents can vary from one study to another. In general, b_1 and b_5 are of order one; b_2 varies from -0.14 (Strahle & Shivashankara 1975) to 0.04 (Strahle 1978); b_3 is suggested to be one in an earlier study (Strahle & Shivashankara 1975) and has been revised to be -1.2 in a later review (Strahle 1978) and b_4 varies from 2 to 3. The values of these exponents depend on how the fluctuating heat release rate is modelled and uses an assumption that the large (integral) scale turbulence is involved in the generation of combustion noise. This assumption is contradicted by an experimental study (Kilham & Kirmani 1979) suggesting that the integral scales have no effect on combustion noise but an increase in turbulent velocity fluctuation increases the combustion noise power in the far field. Note also that no turbulent quantities are involved in the above scaling. The increase in the far-field acoustic power level with the turbulence level is also confirmed by Kotake & Takamoto (1990) for lean-premixed flames. The noise emitted by rich premixed open flames does not seem to be affected by either turbulence level or burner geometry (Kotake & Takamoto 1987, 1990). These useful insights were obtained without addressing the two-point correlation of the rate of change of the fluctuating heat release rate and the associated correlation volume.

As noted by Swaminathan *et al.* (2011) and shown in § 2, this correlation and the associated volume, v_{cor}, are central to combustion noise studies. Different length scales have been suggested in the past to define v_{cor} empirically. Bragg (1963) took the correlation volume to be ${\delta_L^o}^3$, where δ_L^o is the planar laminar flame thermal thickness, by presuming the flame fronts to be locally laminar flamelets and suggested a semi-empirical scaling with $b_3 = b_5 = -1$. Strahle (1971) suggested using $v_{cor} \sim {\delta_L^o}^{3-q} \Lambda^q$, where Λ is the turbulence-integral length scale, for flamelets combustion and deduced a scaling for the acoustic efficiency with $b_3 = b_5 = -1$ and involving $(\Lambda/\delta_L^o)^q$, where the exponent q has to come from experiments. Strahle (1971) also suggested that $v_{cor} \sim \Lambda^3$ when the turbulent combustion occurs in a distributed manner (i.e. low-Da combustion). Hirsch *et al.* (2007) and Wasle, Winkler & Sattlemayer (2005) noted the correlation length scale to be the turbulent flame-brush thickness, δ_t, which is expected to scale with Λ, using chemiluminescence and hydroxyl (OH) planar laser-induced fluorescence (PLIF) techniques. A similar value is reported by Hemchandra & Lieuwen (2010) from chemiluminescence measurements of Rajaram & Lieuwen (2009) and using a theoretical analysis which treated the flame surface to be a passive, propagative and advective interface. A recent study (Swaminathan *et al.* 2011) suggested ${\delta_L^o}^3/8$ for v_{cor}. Despite these propositions, it is still not clear what would be the appropriate length scale for v_{cor} because predicting the far-field combustion noise level from a practical burner is still challenging and unattained as noted by Mahan (1984). Experimental studies addressing this correlation function would be very valuable.

In the present paper, we explicitly show that the combustion noise has two contributions: one from the thermochemical processes and another from the turbulence. This clear distinction has not been made in earlier studies. It has also been shown that the thermochemical processes dictate the two-point correlation. The influences of turbulence come through the mean heat release rate, which cannot be modelled using semi-empirical scaling for well-known reasons. Using these insights, far-field SPL for open turbulent premixed flames of methane– and propane–air mixtures are computed and compared with recent experimental measurements of Rajaram (2007). These flames have a range of turbulence and thermochemical conditions, and heating rate (2–30 kW). However, the spectral content of this far-field sound is not considered in this study as it requires two-point space–time correlations.

The remaining paper is organised as follows. In § 2, (1.1) is briefly derived starting from the Lighthill equation and a discussion on the analysis of the two-point correlation function is presented. The pertinent details of DNS and experimental data used to study the two-point correlation are discussed in § 3. The results are presented in § 4. A brief discussion on the turbulent combustion model (Kolla, Rogerson & Swaminathan 2010) required to calculate the far-field SPL is provided in § 5. The computed results are discussed and compared with experimental measurements in this section. The results of this study are summarised in the last section.

2. Background theory

2.1. *The acoustic sources*

Sound field emitted from a turbulent flame is governed by the wave equation, which is obtained using the mass and momentum conservation equations, as has been originally shown by Lighthill (1952, 1954). This equation, known as the Lighthill equation, for the fluctuating density field, $\rho' = \rho - \rho_o$, is written using the standard nomenclature as

$$\frac{\partial^2 \rho'}{\partial t^2} - a_o^2 \frac{\partial^2 \rho'}{\partial x_i \partial x_j} \delta_{ij} = \frac{\partial^2 T_{ij}}{\partial x_i \partial x_j}, \tag{2.1}$$

where $T_{ij} \equiv \rho u_i u_j - \tau_{ij} + (p' - a_o^2 \rho') \delta_{ij}$ is the Lighthill's stress tensor which includes three components and the fluctuating pressure is $p' = p - p_o$. The Kronecker delta is denoted by δ_{ij}. The first two components are respectively the turbulent and molecular viscous stresses while the third component originates from thermodynamic source. Equation (2.1) can be rearranged to give (Doak 1972; Hassan 1974; Crighton *et al.* 1992)

$$\frac{1}{a_o^2} \frac{\partial^2 p'}{\partial t^2} - \frac{\partial^2 p'}{\partial x_i \partial x_j} \delta_{ij} = \frac{\partial^2}{\partial x_i \partial x_j} (\rho u_i u_j - \tau_{ij}) - \frac{\partial^2 \rho_e}{\partial t^2} \tag{2.2}$$

for the pressure fluctuations, where $\rho_e = \rho' - p'/a_o^2$. Now, the objective is to express $\partial \rho_e / \partial t$ using thermodynamic relations and the specific entropy, s, balance equation as discussed by Crighton *et al.* (1992). The first step is to write

$$\frac{\partial \rho_e}{\partial t} = \frac{\mathrm{D} \rho_e}{\mathrm{D} t} - \frac{\rho_e}{\rho} \frac{\mathrm{D} \rho}{\mathrm{D} t} - \frac{\partial u_i \rho_e}{\partial x_i}, \tag{2.3}$$

using the mass conservation, where $\mathrm{D}/\mathrm{D}t$ is the total or substantial derivative. Then, an expression for $\mathrm{D}\rho/\mathrm{D}t$ is obtained using the balance equation for s and the thermodynamic state relationship $p = p(\rho, s, Y_m)$ for a multi-component reactive mixture, where the mass fraction of species m is denoted by Y_m. The final equation

for the fluctuating pressure is given by (Crighton *et al.* 1992)

$$\frac{1}{a_o^2}\frac{\partial^2 p'}{\partial t^2} - \frac{\partial^2 p'}{\partial x_i \partial x_j}\delta_{ij} = \mathscr{T}_1 + \mathscr{T}_2 + \mathscr{T}_3 + \mathscr{T}_4, \tag{2.4}$$

where

$$\mathscr{T}_1 \equiv \frac{\partial^2}{\partial x_i \partial x_j}(\rho u_i u_j - \tau_{ij}), \quad \mathscr{T}_2 \equiv \frac{\partial^2 \rho_e u_i}{\partial t \partial x_i}, \tag{2.5}$$

$$\mathscr{T}_3 \equiv \frac{1}{a_o^2}\frac{\partial}{\partial t}\left[\left(1 - \frac{\rho_o a_o^2}{\rho a^2}\right)\frac{\mathrm{D}p}{\mathrm{D}t} - \frac{p - p_o}{\rho}\frac{D\rho}{Dt}\right] \tag{2.6}$$

and

$$\mathscr{T}_4 \equiv \frac{\partial}{\partial t}\left[\frac{\rho_o(\gamma - 1)}{\rho a^2}\left(\dot{Q} - \frac{\partial q_i}{\partial x_i} + \tau_{ij}\frac{\partial u_i}{\partial x_j} + \sum_{m=1}^{N} h_m \frac{\partial J_{m,i}}{\partial x_i}\right)\right]. \tag{2.7}$$

Although this equation has been derived explicitly by Crighton *et al.* (1992), a brief derivation is given in Appendix A, outlining the important steps for completeness. The heat release rate per unit volume is $\dot{Q}$, and the heat flux and the molecular diffusive flux of species m in direction i are respectively q_i and $J_{m,i}$, and the enthalpy of species m is h_m.

The terms on the right-hand side of (2.4) represent the various sources of sound generation. The first source is due to flow noise and the second is due to forces resulting from spatial acceleration of density inhomogeneities. The third source is significant when $\rho_o a_o^2 \neq \rho a^2$ and the thermodynamic pressure is time varying and not equal to p_o. The fourth term includes the irreversible sources coming from the rates of changes of the heat release rate, heat transport, viscous dissipation and molecular transports. It has been shown by Flemming *et al.* (2007) and Ihme *et al.* (2009) that the density-related source, $\mathscr{T}_4$, is about two orders of magnitude larger than the other sources for combustion noise from open flames, and thus we shall consider only $\mathscr{T}_4$ in our analysis. Also, the contribution of the heat release rate is far larger than the other three terms in $\mathscr{T}_4$ and thus we shall retain only $\dot{Q}$. If the turbulent combustion occurs in low-Mach-number flows with $p \approx p_o$ as in open flames and the temperature dependence of γ is weak, then (2.4) becomes

$$\frac{1}{a_o^2}\frac{\partial^2 p'}{\partial t^2} - \frac{\partial^2 p'}{\partial x_i \partial x_j}\delta_{ij} = \frac{(\gamma - 1)}{a_o^2}\frac{\partial \dot{Q}(\boldsymbol{y}, t)}{\partial t}. \tag{2.8}$$

An interesting point to note here is that the source for sound generation is the rate of change in the heat release rate. Hence, commonly used Mach number scaling for the acoustic efficiency, η_{ac}, in many earlier studies (see § 1) of combustion noise is not fully justifiable.

By using the Green's function method to solve (2.8), one writes

$$p'(\boldsymbol{r}, t) = \frac{(\gamma - 1)}{4\pi r a_o^2}\frac{\partial}{\partial t}\int_{v_y} \dot{Q}\left(\boldsymbol{y},\, t - \frac{r}{a_o}\right)\mathrm{d}^3 y, \tag{2.9}$$

as its far-field solution when the turbulent flame brush is acoustically compact, i.e., when the wavelength of the emitted sound is large compared to the size of the flame-brush thickness, which is typically taken as the cube root of the volume enclosed by the curve marked as the flame brush in figure 1. Equation (2.9) is exactly the same as (1.1). The variations of γ and the speed of sound inside the flame brush

arising due to temperature inhomogeneities can cause convection and refraction of sound, as noted by Dowling (1976) and Strahle (1973). For simplicity, these effects are neglected as noted earlier. Now it is clear that the combustion noise is generated by the rate of change in the integral of the heat release rate which causes a change in dilatation of the region undergoing turbulent combustion. Thus, the source for combustion noise behaves as a monopole source of sound. Many scaling laws and empirical relations have been proposed in the past (see § 1) to understand the physics of combustion noise. However, these relations have enjoyed limited success (Rajaram & Lieuwen 2003) since they largely depend on the turbulent combustion model used in the analysis, and also many of these relations contradict one another as noted in the Introduction. As noted by Mahan (1984) nearly twenty years ago, the prediction of sound level in the acoustic far-field of a practical burner still remains challenging.

The SPL is characterised by $\overline{p'^2}$, which can be obtained from (2.9). This quantity can be measured in experiments and it is given by (Lighthill 1952)

$$\overline{p'^2}(\boldsymbol{r}) = \frac{(\gamma-1)^2}{16\pi^2 r^2 a_o^4} \int_{v_y} \int_{v_{cor}} \overline{\ddot{Q}(\boldsymbol{y},\, t)\, \ddot{Q}(\boldsymbol{y}+\boldsymbol{\Delta},\, t)}\, \mathrm{d}^3\Delta\, \mathrm{d}^3 y, \tag{2.10}$$

where $\ddot{Q}$ is the temporal rate of change of the fluctuating heat release rate ($\partial \dot{Q}/\partial t$), the separation vector is $\boldsymbol{\Delta}$ and the overbar indicates an averaging process. The symbol v_{cor} denotes the volume over which $\ddot{Q}$ is correlated. Another quantity of interest in combustion noise studies, as noted in the Introduction, is the thermoacoustic efficiency defined by $\eta_{ac} \equiv P_{ac}/(\dot{m}_f H)$, where $\dot{m}_f$ is the fuel flow rate and H is the lower heating value of the fuel. This quantity represents the fraction of the chemical energy released in the combustion process which appears as acoustic energy in the far field. The acoustic power, P_{ac}, is given by $\int_A \overline{p'^2}(r)\, \mathrm{d}A/(\rho_o a_o)$, where $\mathrm{d}A$ is the elemental surface area on a sphere of radius r. Many earlier studies have proposed scaling laws for η_{ac} also, but as one can observe the central quantity is the SPL.

The crux of predicting the far-field SPL accurately and reliably is the treatment and modelling of the two-point correlation appearing in (2.10). The correlation volume, v_{cor}, and the flame-brush volume, v_y, are required accurately. Thus, looking for semi-empirical scaling laws for the acoustic power in terms of burner geometry, mean turbulent flow characteristics and reactant mixture attributes may, perhaps, lead to an oversimplification of the problem. This is because the fluctuating heat release rate and its temporal rate of change strongly depend not only on the turbulence and reactants' characteristics but also on the turbulence–chemistry interaction. It is well known that this interaction is strongly nonlinear and plays a vital role in predicting turbulent combustion in general. Much progress has been made on this topic in the past couple of decades, and we shall avail these developments in our analysis here. The other issue in calculating SPL revolves around the correlation volume, v_{cor}. As noted in § 1, different length scales have been used by various researchers to obtain this correlation volume without investigating the correlation. However, the advent of sophisticated computing techniques and laser metrology enables one to obtain reliable and accurate information on this correlation length scale (Swaminathan *et al.* 2011). Here, the modelling of the two-point correlation in (2.10) is first studied by analysing DNS (Rutland & Cant 1994; Nada *et al.* 2005) and laser diagnostic data (Balachandran *et al.* 2005) of turbulent premixed flames. The results of this analysis are then used along with a recent (Kolla *et al.* 2010) turbulent combustion model for calculating the far-field SPL reported by Rajaram

(2007). The SPL in dB is given by $20\ \log_{10}(p_{rms}/p_{ref})$, where p_{ref} is 2×10^{-5} N m^{-2} and $p_{rms}\equiv\sqrt{\overline{p'^2}}$.

2.2. *Two-point correlations*

It is common to use a progress variable c, varying from zero in the unburnt reactants to unity in the burnt products, for analysing turbulent premixed flames. The progress variable is usually normalised temperature or fuel mass fraction (Poinsot & Veynante 2001) while alternative definitions (Bilger 1993) are possible. The instantaneous progress variable is governed by

$$\rho\frac{\partial c}{\partial t}=\dot{\omega}+\frac{\partial}{\partial x_j}\left(\rho\alpha\frac{\partial c}{\partial x_j}\right)-\rho u_i\frac{\partial c}{\partial x_i}, \tag{2.11}$$

where $\dot{\omega}$ is the chemical reaction rate, α is the diffusivity of c and u_i is the component of fluid velocity in the spatial direction x_i. The second and third terms on the right-hand side of (2.11) denote, respectively, the molecular diffusion and advection processes inside a control volume. The chemical reaction rate $\dot{\omega}$ is directly related to the heat release rate $\dot{Q}$ and the specific form of this relation depends on the detail of the definition of c. If the progress variable is defined using temperature, then the heat release rate is given by $\dot{Q}=c_p(T_b-T_u)\,\dot{\omega}$, where c_p is the specific heat capacity at constant pressure, T_b is the temperature of combustion products and T_u is the temperature of unburnt reactants. If c is based on the fuel mass fraction, then $\dot{Q}=Y_{f,u}\,H\,\dot{\omega}$, where $Y_{f,u}$ is the fuel mass fraction in the unburnt reactants, which is uniform in the premixed case considered here. Because of these simple relations, from here onwards we shall use $\ddot{\omega}$ instead of $\ddot{Q}$ in our analysis.

The time derivative of the fluctuating heat release rate is equal to the time derivative of the instantaneous heat release rate in a statistically stationary turbulent flame and thus $\ddot{\omega}'=\ddot{\omega}$. Using this equality and the above relation between the reaction rate and the heat release rate, the two-point correlation of the rate of change of the fluctuating heat release rate appearing in (2.10) can be written as

$$\left.\begin{aligned}\overline{\ddot{Q}(\boldsymbol{y},\,t)\,\ddot{Q}(\boldsymbol{y}+\boldsymbol{\Delta},\,t)}&=Y_{f,u}^2\,H^2\overline{\ddot{\omega}(\boldsymbol{y},\,t)\,\ddot{\omega}(\boldsymbol{y}+\boldsymbol{\Delta},\,t)},\\ \overline{\ddot{\omega}(\boldsymbol{y}-\boldsymbol{\Delta}/2,\,t)\,\ddot{\omega}(\boldsymbol{y}+\boldsymbol{\Delta}/2,\,t)}&=\Omega_1(\boldsymbol{y},\boldsymbol{\Delta})\,\overline{\ddot{\omega}^2(\boldsymbol{y},\,t)},\end{aligned}\right\} \tag{2.12}$$

where Ω_1 is the correlation function for statistically stationary flames. This correlation function and $\overline{\ddot{\omega}^2}$ are independent of the time, t. Note that this correlation function may depend on the spatial location $\boldsymbol{y}$ in the flame and may be different in different spatial directions. However, the correlation function is observed to be independent of the spatial location and to depend only on the separation distance, $\Delta=|\boldsymbol{\Delta}|$, discussed in § 4.

One needs a closure model for $\overline{\ddot{\omega}^2}$ while computing SPL and this model is obtained in the following manner by writing $\overline{\ddot{\omega}^2}=\mathscr{B}_1^2\,\overline{\dot{\omega}'^2}$, where $\mathscr{B}_1$ is the inverse of a time scale, on an average, for the rate of change of the fluctuating reaction rate. One can also relate the root-mean-square (r.m.s.) value of the reaction rate fluctuations to its mean value by $\sqrt{\overline{\dot{\omega}'^2}}=\mathscr{B}\overline{\dot{\omega}}$, which can be obtained simply

$$\overline{\dot{\omega}'^2}\;=\;\overline{(\dot{\omega}-\overline{\dot{\omega}})^2}\;=\;\overline{\dot{\omega}}^2\left(\frac{\overline{\dot{\omega}^2}}{\overline{\dot{\omega}}^2}-1\right)\;=\;\mathscr{B}^2\,\overline{\dot{\omega}}^2. \tag{2.13}$$

The definition of $\mathscr{B}$ and its meaning are evident from the above equation. It is well known that the reaction rate signal in turbulent flames is highly intermittent in space

as well as in time. The r.m.s. value of such signals can be as high as or even larger than the mean value and this has been shown in Appendix B. This implies that $\mathscr{B}$ can be of order one in highly turbulent flames as one shall observe in § 4 and it is also expected that $\mathscr{B}$ will be less sensitive to turbulence characteristics. The two-point correlation can now be simply written as

$$\overline{\ddot{\omega}(\boldsymbol{y}-\boldsymbol{\Delta}/2,\,t)\,\ddot{\omega}(\boldsymbol{y}+\boldsymbol{\Delta}/2,\,t)} = \mathscr{K}^2\,\Omega_1(\Delta)\,\overline{\dot{\omega}(\boldsymbol{y},\,t)}^2, \tag{2.14}$$

where $\mathscr{K}$ is equal to $\mathscr{B}_1\mathscr{B}$. Substituting (2.14) for the heat release rate correlation in (2.10), the expression for the far-field SPL is obtained simply as

$$\overline{p'^2}(\boldsymbol{r}) = \frac{(\gamma-1)^2}{16\pi^2 r^2 a_o^4}\,Y_{f,u}^2\,H^2\,\underbrace{\int_{v_y}\mathscr{K}^2\,\overline{\dot{\omega}(\boldsymbol{y},\,t)}^2}_{\text{turbulence}}\;\underbrace{\int_{v_{cor}}\Omega_1(y,\,\Delta)\,\mathrm{d}^3\Delta}_{\text{thermochemical}}\,\mathrm{d}^3 y, \tag{2.15}$$

where the expected contributions from the thermochemistry and turbulence are noted. The inverse of the time scale for the rate of change of the heat release rate fluctuation can vary spatially inside the flame brush and thus the parameter $\mathscr{K}$ is kept inside the first integral. However, the other parameter $\mathscr{B}$ is expected to be a constant of order unity as one shall see in § 4. The second integral is over the correlation volume, which is observed to be independent of the position inside the flame brush (see § 4.3), i.e. $\Omega_1(y,\,\Delta) = \Omega_1(\Delta)$. Hence, the second integral can be evaluated independently once the correlation function Ω_1 is known. As far as the mean heat release rate is concerned, any sensible model can be used. However, applying semi-empirical scaling laws is not advisable because the mean heat release rate and the flame-brush volume, required for the integration, depend not only on the gross characteristics of burner, turbulence and fuel reactivity but also on the interaction of turbulence and chemical reactions. It is well known that this nonlinear interaction is difficult to capture using scaling laws.

Similar to the two-point correlation for $\ddot{\omega}$, one can also write a two-point correlation for the heat release rate fluctuation as

$$\overline{\dot{\omega}'(\boldsymbol{y}-\boldsymbol{\Delta}/2,\,t)\,\dot{\omega}'(\boldsymbol{y}+\boldsymbol{\Delta}/2,\,t)} = \Omega(\boldsymbol{y},\,\boldsymbol{\Delta})\,\overline{\dot{\omega}'^2(\boldsymbol{y},\,t)}, \tag{2.16}$$

using another correlation function Ω. It has been shown by Swaminathan *et al.* (2011) that exponential functions can represent these correlation functions reasonably well and the planar laminar flame thermal thickness can be used to scale correlation length scales. The two questions we ask for this study are (i) is there an influence of fuel type, stoichiometry and flame Damköhler and Reynolds numbers on these correlation functions? and (ii) are the correlation length scale ℓ for the fluctuating reaction rate and ℓ_1 for the rate of change of the fluctuating reaction rate related?, if so, how? The second question is important from the experimental point of view. Although an attempt has been made by Wasle *et al.* (2005) to measure the correlation length scale ℓ_1, it is relatively easy and less expensive to measure ℓ. This is because deducing information about ℓ_1 requires measurement of the temporal rate of change of the fluctuating heat release rate, which is not an easy quantity to measure reliably. We seek answers to the above questions by detailed analysis of turbulent premixed flame data obtained from the DNS (Rutland & Cant 1994; Nada, Tanahashi & Miyauchi 2004; Nada *et al.* 2005) and laser diagnostics (Balachandran *et al.* 2005) before embarking on the task of calculating the far-field SPL.

Flame	Fuel/chemistry	ϕ	u_{rms}/s_L^o	Λ/δ	Re	Da
R1	Hydrocarbon/single-step	–	1.4	28.3	57	20.1
R2a	H_2/multi-step	1.0	0.85	78.0	107	91.8
R2b	”	”	1.7	39.0	107	22.9
R2c	”	”	3.4	19.5	107	5.7
R2d	”	”	3.4	41.5	190	12.3
R2e	”	”	5.76	56.8	442	9.9
R3a	”	0.6	2.2	34.5	143	15.7
R3b	”	”	4.3	36.7	298	8.5

TABLE 1. Attributes of DNS flames.

3. Attributes of flame data and their processing

3.1. *DNS flames*

The important attributes of eight DNS data sets considered for the two-point correlation analysis are given in table 1. All these cases considered the propagation of a premixed flame in three-dimensional homogeneous turbulence with inflow and outflow boundary conditions in the mean flame propagation direction. The other two spatial directions were specified to be periodic. These boundary conditions mimic the situations of an open flame. Experimentally, this situation corresponds to an open flame propagating in grid turbulence, which is inherently unsteady. In the run R1 (Rutland & Cant 1994), a single irreversible reaction with large activation energy was used and fluid properties were taken as temperature independent. The thermochemical parameters used were representative of hydrocarbon combustion. In the set of R2 and R3 runs, turbulent premixed combustion of stoichiometric and lean (equivalence ratio of $\phi = 0.6$) hydrogen–air mixtures were simulated (Nada *et al.* 2004, 2005) using a detailed kinetic mechanism involving 27 reactions and 12 reactive species. The variation of fluid properties with temperature was included using CHEMKIN packages and the reactant mixture was preheated to alleviate numerical stiffness problems. A range of fluid dynamic conditions considered are shown in table 1. The r.m.s. of turbulence velocity fluctuation and its integral length scale are respectively denoted by u_{rms} and Λ in table 1. The Zeldovich thickness for the laminar flame is $\delta \equiv \alpha_u/s_L^o$, where α_u is the thermal diffusivity of the unburnt mixture. The turbulence Reynolds number is defined as $Re \equiv u_{rms}\Lambda/\nu_u$, with ν_u being the kinematic viscosity of the unburnt mixture. The Damköhler number is

$$Da \equiv \frac{t_f}{t_c} = \frac{(\Lambda/\delta)}{\left(u_{rms}/s_L^o\right)}, \tag{3.1}$$

where t_f is the turbulence integral time scale and t_c is the chemical time scale. In all the DNS cases, the two-way coupling between the turbulence and chemistry was retained by allowing the density to vary spatially and temporally.

The values of Re and Da in table 1 indicate that these flames span from the wrinkled flamelets to the thin reaction zones in the combustion regime diagram of Peters (2000), which is shown in figure 2. The conditions of experimental flames discussed later are also marked in this figure as EFs and IDs. Note that the conditions of the numerical and experimental flames are complementary to one another and they together cover a wide range of combustion conditions. Also, they provide complementary information for this study.

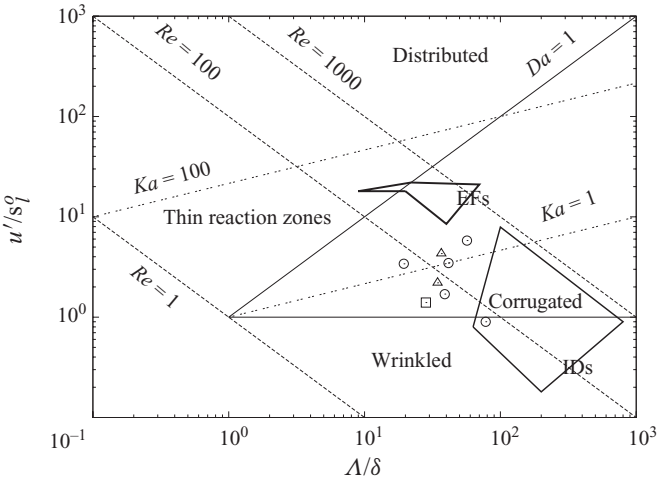

FIGURE 2. Turbulent combustion regime diagram showing conditions of DNS (square, R1; circles, set R2; triangles, set R3) and experimental flames (Balachandran *et al.* 2005), marked as region EFs, considered for the two-point correlation analysis. The other experimental flames (Rajaram 2007; Rajaram & Lieuwen 2009) in the region marked as IDs are used for the SPL calculation.

The DNS data at about 4.4 initial eddy turnover time, which correspond to about 19 flame time, from the run R1 are considered for analysis. From the set of R2 and R3 simulations, the DNS data at about 2.5 initial eddy turnover time are used. This corresponds to a minimum of about 14 flame time, which is for the simulation R2c. The numerical resolution is found to be more than adequate to resolve the thin flame front structure and the turbulence characteristics in all cases. Furthermore, the size of time steps used in the simulations is much smaller than the smallest time scale involved, which is usually associated with the combustion chemistry. All the simulations were run long enough to attain nearly a fully developed state for combustion and its interaction with turbulence. This state may be viewed as an approximate statistical stationary state since the mean burning rate in the computational volume remains fairly constant. Complete details on the DNS can be found elsewhere (Rutland & Cant 1994; Nada *et al.* 2004, 2005). It is deemed here that these sets are suitable for analysing the two-point correlations, Ω and Ω_1.

The construction of the two-point correlation Ω for the reaction rate fluctuation is a straightforward exercise, whereas the calculation of Ω_1 requires the temporal derivative, which is usually unavailable in the common practice of storing primitive variables, such as velocities and temperature, at discrete time levels in direct simulations. This difficulty is overcome in the following manner. If a single-step reaction with a rate expression of the form

$$\dot{\omega} = A\,\rho(1-c)\exp\left[\frac{-\hat{\beta}(1-c)}{1-\hat{\alpha}(1-c)}\right] \tag{3.2}$$

is used to model the combustion chemistry, as has been done in the simulation R1, then one can write $\ddot{\omega} = (\mathrm{d}\dot{\omega}/\mathrm{d}c)\,(\partial c/\partial t)$. The symbol A denotes the pre-exponential

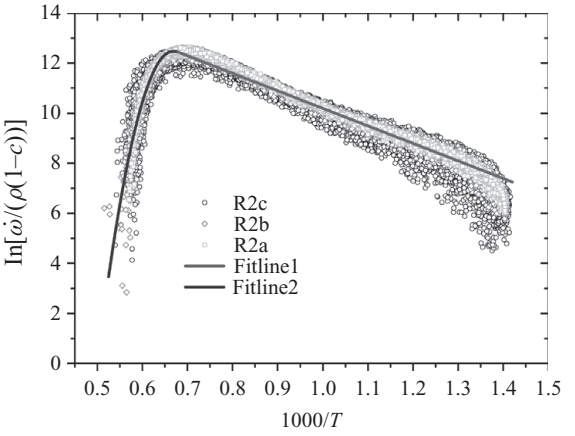

FIGURE 3. Typical Arrhenieus plot from the DNS results. The fits of (3.4) (Fitline1) and (3.5) (Fitline2) are also shown by solid lines.

factor and the parameters $\hat{\beta}$ and $\hat{\alpha}$ are, respectively, given by

$$\hat{\beta} = \frac{T_a}{T_u}\frac{\tau}{(1+\tau)^2} \quad \text{and} \quad \hat{\alpha} = \frac{\tau}{1+\tau}, \tag{3.3}$$

where T_a is the activation temperature and τ is the temperature rise across the flame front normalised by the reactant temperature. The density, ρ, can be related to c based on temperature via the state equation, which is given by $\rho = \rho_u/(1+\tau\, c)$. By replacing $\partial c/\partial t$ using (2.11), one can see that $\ddot{\omega}$ can be obtained using the DNS data stored at discrete time levels and their spatial derivatives. Strictly speaking, this method is applicable only if the rate expression of the above form is used and the rate of mass diffusion is equal to the rate of heat diffusion. The rate of change of the heat release rate obtained thus is used to construct Ω_1 for the simulation R1, since this simulation satisfies all of these conditions. It is ideal to calculate and store $\ddot{\omega}$ when the DNS is run but, in the absence of such information, it is inevitable to resort to alternative methods such as proposed above.

One can, in principle, follow this approach to get $\ddot{\omega}$ in general but the algebra becomes intractable when a complex chemical kinetics mechanism is used, as in the simulation sets R2 and R3. For these simulations, one can create an Arrhenieus-type plot using the local reaction rate, density, temperature and fuel mass fraction to obtain rate constants in (3.2). The progress variable is defined using the fuel mass fraction. Such a plot is shown in figure 3 for three simulations R2a, R2b and R2c. There is good collapse of the data into two different regions. Thus, a single fit is not possible, and also if one uses two different linear fits then there would be a discontinuity in the slope at about 1540 K. Thus, a least-squares fit of the form $\dot{\omega} = \rho(1-c)\exp[G(T)]$ is sought with

$$G(T) = \hat{b}_0 + \hat{b}_1/T, \qquad \text{for } T < 1540 \text{ K}, \tag{3.4}$$

$$= \hat{b}_3 + \hat{b}_4/T + \hat{b}_5/T^2, \qquad \text{for } T \geqslant 1540 \text{ K}, \tag{3.5}$$

where $\hat{b}_i$ values are the least-square fit parameters. These two fits are shown by solid lines in figure 3 and their agreement with the data is good. Depending on the local temperature, one of these two fits is used to obtain $\ddot{\omega}$ following the above procedure.

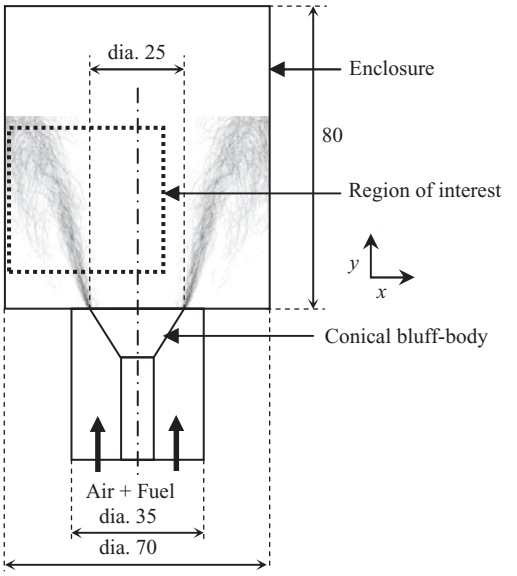

FIGURE 4. Schematic diagram of the bluff-body burner set-up. All dimensions are in mm.

3.2. *Experimental flames*

Since the DNS is usually limited to low Re, as one can see in table 1, because of the numerical resolution required and the associated computational cost for high Re, the DNS data analysis is complemented with the analysis of laser diagnostic data from experiments of bluff-body-stabilised turbulent lean-premixed flames. These flames and the bluff-body burner have been the subject of various experimental (Balachandran *et al.* 2005), theoretical (Hartung *et al.* 2008) and computational (Armitage *et al.* 2006) studies addressing different aspects of turbulent lean-premixed flames. Complete details of the burner and experimental procedure can be found in Balachandran *et al.* (2005) and Ayoola *et al.* (2006). However, a brief discussion on the burner, flow conditions and experimental method is provided.

The burner consists of a 300 mm long circular duct of inner diameter 35 mm with a conical bluff body of diameter 25 mm giving a blockage ratio of 50 %, which stabilises the flame. Figure 4 shows the schematic diagram of the close-up of the bluff-body arrangement. After appropriate flow conditioning, the premixed reactants were allowed through the annular region as shown in figure 4. Ethylene fully premixed with the air upstream of the burner was used as the reactant. The flame was enclosed using a 80 mm long fused silica quartz cylinder of inner diameter 70 mm, which provided optical access for PLIF imaging and also avoided a change in equivalence ratio (ϕ) due to possible air entrainment from the surrounding. Four turbulent premixed flames of equivalence ratio 0.52, 0.55, 0.58 and 0.64 with a bulk velocity of 9.9 m s^{-1} at the combustor inlet are considered here. This bulk velocity gives a Reynolds number, Re_d, of about 19 000 based on the bluff-body diameter. These flames are different from those reported by Swaminathan *et al.* (2011), who considered the effects of flow Reynolds number on the two-point correlation of the fluctuating heat release rate. Although the range of ϕ considered here seems narrow, it must be noted that the planar laminar flame speed (Egolfopoulos, Zhu & Law 1990) varies by nearly 100 % over this range of ϕ and lean mixtures are used because of the interest in lean-burn systems for future engines.

Since the interest is on the two-point spatial correlation of the heat release rate, one needs to simultaneously image hydroxyl (OH) and formaldehyde (CH_2O) radicals, because the product of these two signals on pixel-by-pixel basis is shown to correlate well with the local heat release rate for fully premixed flames by Najm *et al.* (1998), Balachandran *et al.* (2005) and Ayoola *et al.* (2006). The accuracy and applicability of this technique are discussed in those references. The arrangement of laser optics for simultaneous OH and CH_2O PLIF imaging is discussed by Balachandran *et al.* (2005) and Ayoola *et al.* (2006) and the measurements were performed with a projected pixel resolution of 35 μm per pixel. After appropriate image corrections and resizing noted by Balachandran *et al.* (2005), the heat release rate image obtained had an effective spatial resolution of 70 μm. The laminar flame thermal thickness for the ethylene–air mixtures considered here ranges between 450 and 540 μm and therefore the resolution employed was sufficient to resolve the details of the heat release rate variation within instantaneous flame front.

Figure 4 shows the region of interest for the PLIF measurements, which is about 40 mm × 25 mm (width × height) and is located at about 5 mm above the bluff body and about 4 mm from the enclosure wall. After incorporating a number of corrections to minimise contributions from background noise, shot-to-shot variation in laser irradiance, variation in beam profile, both OH and CH_2O images were overlapped on a pixel-by-pixel basis to obtain a quantity that is proportional to the local heat release rate. These images, referred to as reaction-rate images, are further processed to obtain the correlation function, Ω, required for this study. Since single shot imaging was done in the experiments, deducing information about Ω_1 is not possible. The experimental results on Ω are mainly used to corroborate the DNS findings. Uncertainties in the heat release estimation are discussed in detail by Balachandran *et al.* (2005) and Ayoola *et al.* (2006). In order to further understand the effects of these errors in the estimation of the heat release rate on the correlation function, additional analyses are performed as described below. A random noise having a magnitude of about $\pm 10\,\%$ of the local value is added to the instantaneous heat release rate images and then these images are used to calculate Ω. A comparison of Ω obtained using the images without and with noise included indicates that these correlation values differ only by about 5 %. Note also that Ω dropped to zero from unity quicker when noise was added and a difference of about 10 % is noted in the separation distance to reach $\Omega = 0.05$.

The local conditions of the turbulent combustion are expected to be in the thin reaction zones regime marked as EFs in figure 2 based on the results reported by Hartung *et al.* (2008). Despite the complementary combustion conditions in the DNS and experimental flames as shown in this figure, nearly the same behaviour of Ω is observed for these flames as noted in § 4.2.

4. Result and discussion

4.1. *General flame features*

The three-dimensional iso-surface of $c = 0.5$ at $t^+ = 19.4$ is shown in figure 5 from the simulation R1. The reactants enter the computational domain through $x^+ = 0$ boundary plane and the hot products leave through the $x^+ = 38$ plane. Here and in the following discussion, the quantities with superscript + denote values appropriately normalized using the unstrained planar laminar flame thermal thickness, its propagation speed and the unburnt mixture density. The contours of $\dot{\omega}$ and $\ddot{\omega}$ are also shown in this figure. The level of corrugation and contortion of the iso-surface

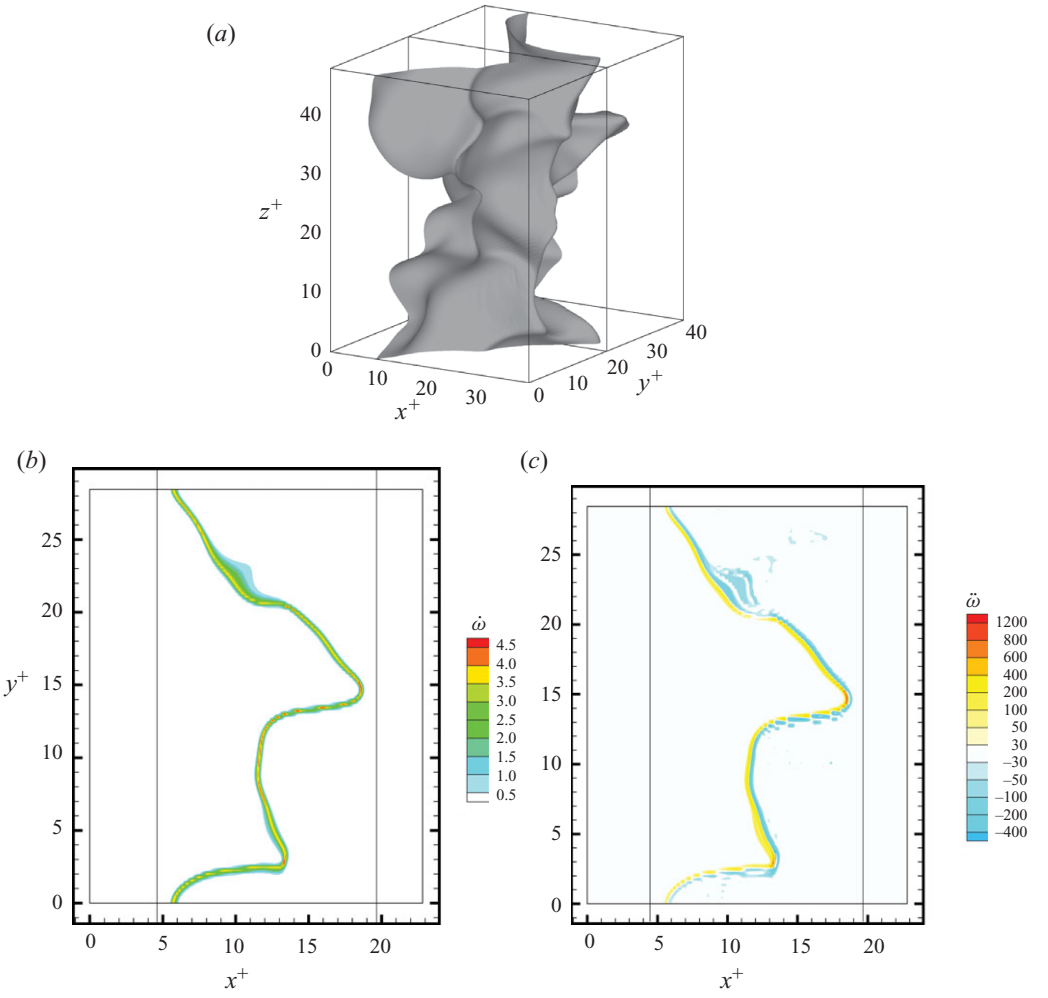

FIGURE 5. (*a*) Instantaneous iso-surface of $c = 0.5$ from simulation R1. Contours of $\dot{\omega}^+$ and $\ddot{\omega}^+$ from simulation R1 for an arbitrary x–y plane are shown in (*b*) and (*c*), respectively. The two vertical lines in (*b*) and (*c*) indicate the edges of the flame brush.

shown in figure 5(*a*) indicates considerable interaction of turbulence with the initial laminar flame. The turbulent flame brush is statistically planar for all the cases in table 1 because of periodic boundary conditions in the cross-stream and spanwise directions and thus the averages are constructed by ensemble averaging in a selected y–z plane. The Favre- or density-weighted average of c, denoted by $\widetilde{c}$, constructed thus is uniquely related to x in these flames because of their statistically one-dimensional nature. Hence, in the following discussion, $\widetilde{c}$ is used to denote the spatial position inside the flame brush unless noted otherwise. The data sample for the analysis is collected by restricting c in the range $0.1 \leqslant c \leqslant 0.9$ to have meaningful statistics since the reaction rate, $\dot{\omega}$, becomes small when the values of c are beyond this range.

The instantaneous reaction rate contours in an arbitrary x–y plane are shown in figure 5(*b*). The normalised reaction rates are confined to thin regions and the flame front is contorted by the turbulence. Also, spatially intermittent nature of $\dot{\omega}^+$ can be

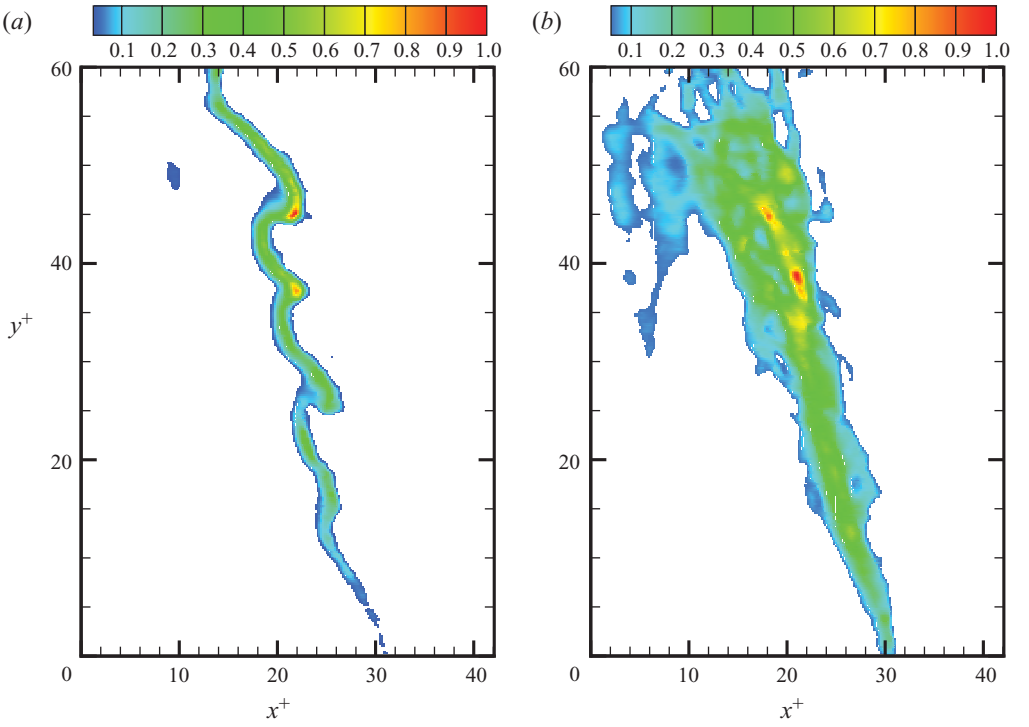

FIGURE 6. Colour map of the instantaneous (*a*) and averaged (*b*) reaction rates from the experimental flame (Balachandran *et al.* 2005) having $\phi = 0.64$. The reaction rates are normalised using the respective maximum values and the distances x and y are normalised using the laminar flame thermal thickness.

observed in this figure. The rate of change of the reaction rate, $\ddot{\omega}$, normalised using the planar laminar flame scales is shown in figure 5(*c*), and this quantity is obtained as explained in § 3.1. The correspondence of $\dot{\omega}^+$ and $\ddot{\omega}^+$ is clear and $\ddot{\omega}$ is confined to a thinner region as in figure 5(*c*). There are two strands of very large values separated by a very thin region having zero value. This is because $\mathrm{d}\dot{\omega}/\mathrm{d}c = 0$ in the region of peak reaction rate (high-valued regions in figure 5*b*). These contours are results of two contributions, (i) $\mathrm{d}\dot{\omega}/\mathrm{d}c$, which will be zero near the location of maximum $\dot{\omega}$ denoted by c^* (for example, $c^* = 0.7$ for the simulation R1), positive for $c < c^*$ and negative for $c > c^*$ and (ii) $\partial c/\partial t$, which includes the contributions from physical processes, viz. chemical reactions, molecular diffusion and the convection (see (2.11)). The rate of change of the fluctuating heat release rate calculated thus will include contributions from all the relevant physical processes. Also, one can expect that the regions with high values of $\ddot{\omega}$ to be thinner than the reaction zones, which is apparent in figure 5(*b*). A similar behaviour of $\dot{\omega}$ and $\ddot{\omega}$ is observed in other cases listed in table 1.

As noted in § 3.2, the product of simultaneous OH and CH_2O PLIF signals on a pixel-by-pixel basis gives a quantity which is proportional to the local instantaneous heat release rate. A typical instantaneous variation of this quantity is shown in figure 6(*a*), where the values are normalised using the maximum observed in this image. The spatial dimensions, x and y, are normalised using the unstrained planar laminar flame thermal thickness, δ_L^o. The flame front is wrinkled by turbulence and

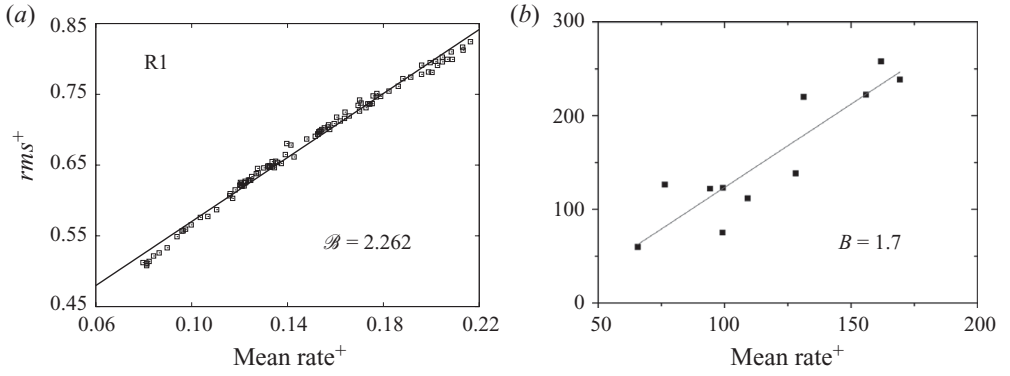

FIGURE 7. Dependence of $\sqrt{\overline{\dot{\omega}'^2}}$ on the mean reaction rate $\overline{\dot{\omega}}$ in the DNS (a) and experimental (b) flames.

the typical thickness of this front is about two thermal thicknesses, except for strongly curved regions. The flame interactions observed by Swaminathan *et al.* (2011) are absent here because the Reynolds number, Re_d, is nearly 2.5 times smaller. A similar observation is made in other images collected for the flame shown in figure 6(a) as well as for flames of other equivalence ratios considered in this study. There were about 75–100 images collected for each equivalence ratio, which were averaged to obtain the spatial variation of the average heat release rate in each flame. A typical spatial variation is shown in figure 6(b) for the $\phi = 0.64$ flame and the values are normalised using the maximum value in the averaged image. The thickness of this averaged heat releasing region in the near field ($y^+ \leqslant 30$) is nearly three to four times thicker than the instantaneous flame front shown in figure 6(a). The turbulent diffusion increases this thickness further at downstream locations as in figure 6(b). Since the turbulence level in the experiments is larger than in the DNS cases as noted in figure 2, the experimental flame fronts are thicker than the numerical cases. Despite this notable difference due to combustion conditions (see figure 2) of the numerical and experimental flames, a similarity in the turbulent flame front behaviour can be observed by comparing figures 5(b) and 6(a).

The reaction rate fluctuations required to construct the two-point correlation, Ω, are obtained by subtracting the mean value from the instantaneous values on point-by-point basis in both the experimental and numerical flames. These fluctuations are then used to obtain the two-point correlation Ω given in (2.16). Before discussing this result, the approximation $\sqrt{\overline{\dot{\omega}'^2}} \approx \mathscr{B}\overline{\dot{\omega}}$ introduced via (2.13) is evaluated. Figure 7(a, b) shows typical variation of the reaction rate fluctuation r.m.s. with the mean reaction rate in the DNS, R1 and experimental flames, respectively. Although the results are shown for simulation R1, it is to be noted that this variation in other simulations is similar to that shown here. Each data point in this figure corresponds to different locations inside the flame brush. The spatial locations of the experimental points are chosen arbitrarily in the range $10\delta_L^o \leqslant y \leqslant 55\delta_L^o$ and $15\delta_L^o \leqslant x \leqslant 30\delta_L^o$. The straight line in figure 7 is the least square fit for the data. The linearity between the r.m.s. and the mean is observed to be good and the parameter $\mathscr{B}$, which may be interpreted as reaction rate intensity (fluctuation amplitude normalised by the mean), varies very little spatially as indicated by small deviations of the data point from the straight line fit. The values of $\mathscr{B}$ obtained from the least-squares fit given in this figure are of order one, as has been asserted in § 2.2.

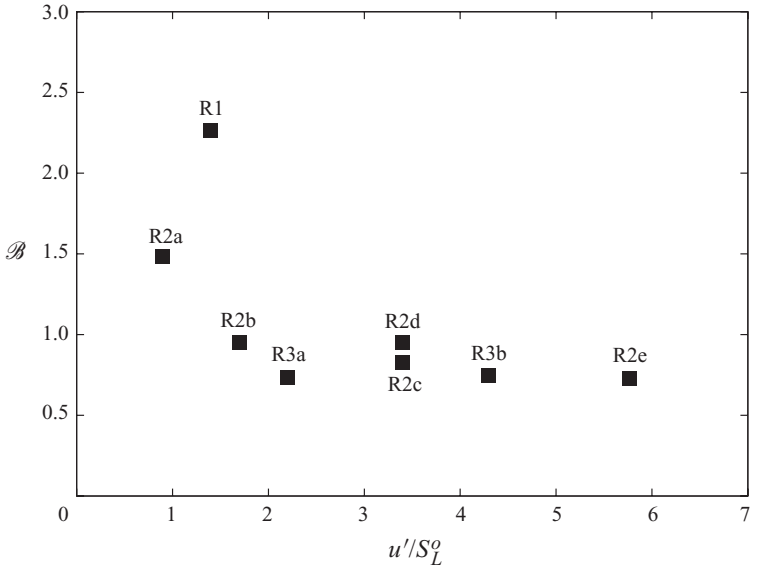

FIGURE 8. Variation of $\mathscr{B}$ with turbulence level in the DNS flames.

Figure 8 shows that the value of $\mathscr{B}$ does not seem to vary much with the turbulence level, at least for the range considered for the DNS flames. This behaviour is expected as noted in § 2.2. A slightly larger value of $\mathscr{B}$ in the simulation R1 is because of the low turbulence Reynolds number (see table 1). However, the experimental value is markedly different from the seemingly converged value in figure 8 from the DNS flames. This is because the reaction intensity increases due to the increase in the spatial intermittency of the reaction zone as noted in § 2.2. Also, the turbulence in the DNS decays spatially like the grid turbulence, but in the experiment the turbulence is produced via the shear, implying that u_{rms} will increase from the burner face. Because of these reasons, the value of $\mathscr{B}$ is taken to be 1.5 in calculations of the far-field sound pressure levels in § 5.

4.2. *Correlation of the reaction rate fluctuation*

The correlation function Ω for the reaction rate fluctuation is calculated using $\dot{\omega}'$ obtained as explained above and the averaging is done in the homogeneous directions for the DNS flames. Thus, the separation distance spans only one direction (x in figure 5*a, b*) for these flames. It is also to be noted that the singular behaviour of Ω, which is not defined outside the flame brush (see (2.16)), is avoided by considering the data in the range $0.1 \leqslant c \leqslant 0.9$ so that the reaction rate fluctuation is not close to zero. For the experimental flames, ensemble averaging is used since the flame brush is not statistically one-dimensional. First, the local maximum of $\dot{\omega}(x, y)$ is identified in the mean image for a given x or y location (see figure 6). The separation distances Δ_x and Δ_y are taken from the point of local maximum, denoted by (x_o, y_o), to construct the two-point correlation functions Ω_x and Ω_y. This ensures that the calculated Ω is physically meaningful. It is observed in the analysis that Ω_x and Ω_y are almost identical for the flames considered for this study and thus one can combine them by using $\Delta^2 = \Delta_x^2 + \Delta_y^2$. Hence, the variation of Ω in the experimental flames is shown using $\Delta = |\boldsymbol{\Delta}|$, normalised by the respective laminar flame thermal thickness.

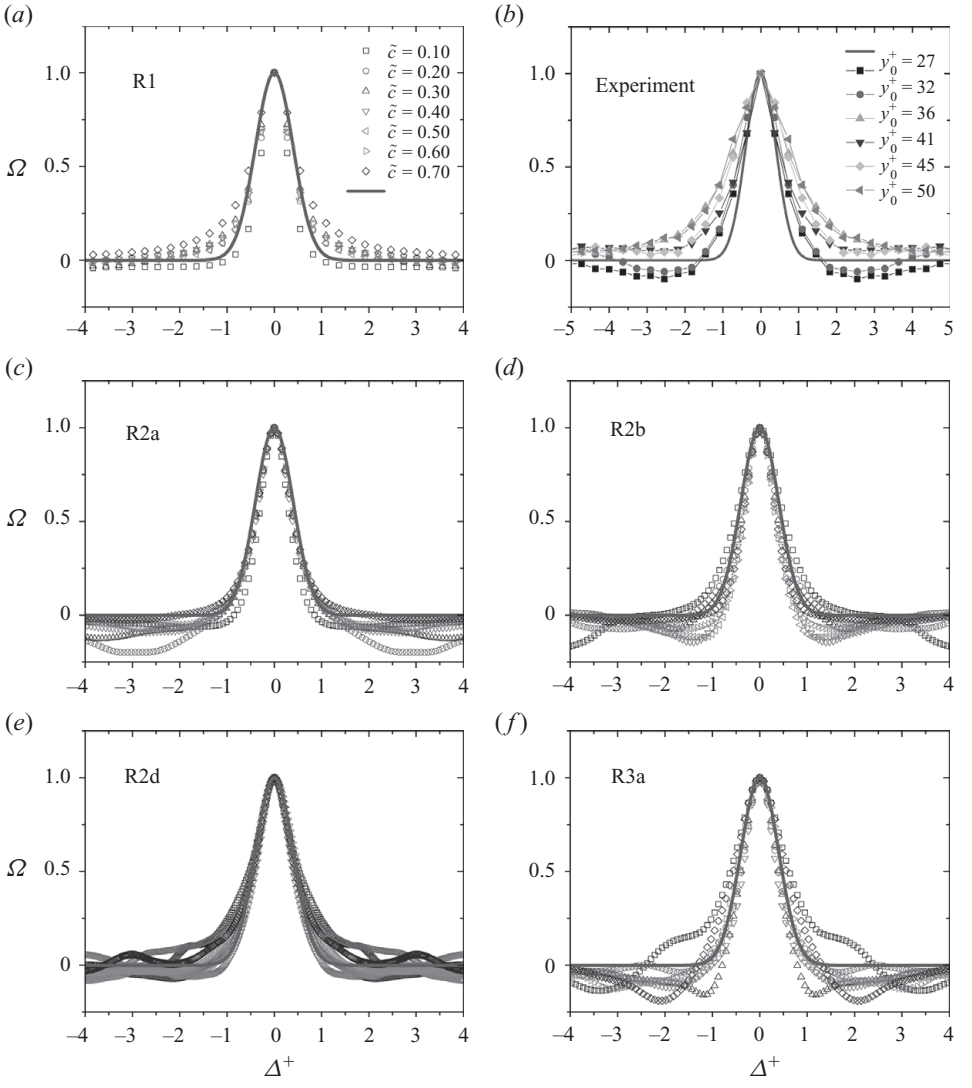

FIGURE 9. (*a–f*) Correlation function, Ω, for the fluctuations in the heat release rate from six different DNS cases and the experimental flame. The solid lines denote the fit using the exponential function $\exp(-\kappa^2 \Delta^{+2})$.

The results are shown in figure 9 for five cases of the numerical flames, which are chosen to elucidate the effects of (i) fuel type (hydrocarbon versus hydrogen), (ii) the equivalence ratio, ϕ, (iii) the velocity ratio u_{rms}/s_L^o and (iv) the length scale ratio Λ/δ_L^o on the two-point correlation function Ω. A typical result for the experimental flames is also shown in this figure for the $\phi = 0.64$ case. The correlation function is shown for seven different locations, denoted by $\widetilde{c}$, inside the numerical flame brushes. For the experimental flame, results from six different streamwise locations are shown. The results for the numerical cases R1 and R2d from our previous study (Swaminathan *et al.* 2011) are included in figure 9 to make the comparison easier.

The separation distance Δ is normalised using the respective unstrained planar laminar flame thermal thickness, δ_L^o. The correlation function Ω is symmetric in all

the flames investigated in this study and its value drops quickly from 1 to about 0.05 over a distance of about 1–2 thermal thickness, δ_L^o, of the respective laminar flames. The reaction rate contours in figures 5(b) and 6(a) clearly show that the flames are thin and thus their dynamics and fluctuation levels are predominantly controlled by the small-scale turbulence, and the large-scale turbulence simply wrinkles the flame front. Thus, it is not surprising to see such a sharp fall of the correlation function. This is also supported by the experimental flames considered here, as can be clearly seen in figure 9. The results shown in figure 9 for the R1-DNS and experimental cases are for hydrocarbon–air flames, whereas the other four cases shown are for hydrogen–air flames. These results show that the two-point correlation function for the fluctuating heat release rate is remarkably similar for these flames, suggesting that the fuel type has negligible influence. A closer study of these results suggests a small variation in the behaviour of this correlation function within the flame brush in the numerical flames; the function becomes slightly broader as one moves towards the burnt side (higher $\widetilde{c}$ values). This change is apparent in the simulation R1 and in the lean hydrogen case R3a because the r.m.s. value $\sqrt{\overline{\dot{\omega}'^2}}$ drops quickly with $\widetilde{c}$ in these two simulations compared to the stoichiometric hydrogen–air flames (specifically, compare R3a and R2b cases shown in figure 9). Also, a comparison of the R2d and R3a cases, which have a similar value of Re and Da as noted in table 1, suggests that the stoichiometry of the reactant mixture has no substantial influence on the behaviour of this correlation function. A similar behaviour is observed in the experimental flames as well.

The numerical flames R2b and R2d have a close value for Λ/δ and different u'/S_L^o values as noted in table 1. Hence, a comparison of the correlation function from these two flames will show the influence of the velocity ratio. The results shown in figure 9 clearly depict that the influence of the velocity ratio is negligibly small. To study the influence of the length scale ratio, one may compare the results of flames R2c (not shown) and R2d, which have the same velocity ratio. This length scale and velocity ratios can be expressed in terms of turbulence Reynolds and Damköhler numbers. The flames R2a, R2b and R2c have the same values of Re but different Da, and one may conclude that the influence of Da is also negligible by comparing the results of R2a and R2b shown in figure 9. Thus, an important point to be noted is that the two-point correlation function for the reaction rate fluctuation is not influenced by the fuel type, stoichiometry, turbulence Reynolds number and Damköhler number if the separation distance is normalised using the planar laminar flame thermal thickness, at least for the range of conditions considered for the numerical flames investigated in this study.

Similar observations are also made in the experimental flames. The experimental flame front at downstream locations denoted by y^+ experiences different turbulence levels (Hartung *et al.* 2008) and thus the combustion conditions are expected to vary from the thin reaction zones to the distributed reaction zones marked in figure 2, which is reflected in the slight broadening of the two-point correlation Ω. Despite this broadening, the sharp fall of Ω from 1 to 0.05 within about two thermal thicknesses remains unchanged. The influence of the statistical sample size (75–100 frames) on the peak and width of Ω is observed to be small by halving the sample size. Note also that there is no turbulence-generating device in the burner and the fluctuations in the velocity field are generated via the shear production mechanism as noted earlier. Furthermore, the effects of the Reynolds number, Re_d, and swirl were shown to be negligible (Swaminathan *et al.* 2011) by using data for different experimental conditions from the burner used in this study.

From the results presented in figure 9 for a wide range of local thermochemical and turbulence conditions, a striking similarity in Ω behaviour is observed. This behaviour can be approximated reasonably well by an exponential function of the form $\exp(-\kappa^2\Delta^{+2})$ for turbulent flames having the thermochemical characteristics of lean hydrocarbon flames. The value of κ giving a best fit to the data cloud is $\sqrt{\pi}$ and also

$$\int_{-\infty}^{\infty} \exp(-\kappa^2\Delta^{+2})\,\mathrm{d}\Delta^{+} = 1. \tag{4.1}$$

This fit does not seem to be so good for hydrogen–air flames and the experimental case because of small negative values of the correlation function. However, the level of agreement seen in figure 9 is acceptable.

As noted earlier, the separation distance Δ spans only one spatial, the mean flame propagation, direction in the numerical flames. Ideally, one would also like to construct the correlation function with separation distance in other two directions. This is possible if one runs the DNS with different set of random numbers to generate turbulence with similar mean attributes and then ensemble average over these DNS runs, which would be a very expensive exercise. However, some knowledge on the likely variation of the correlation function in the other two directions can be gained by studying the reaction rate contours and iso-surface shown in figure 5. The reaction rate contour clearly shows that the flame front is thin and thus the fluctuations of the reaction rate will vary over these thin regions. Hence, one can expect that the correlation function will fall off sharply along the y-direction in a fashion similar to that shown in figure 9. From the level of corrugations and contortions of the iso-surface in the z-direction shown in figure 5(a), it is quite natural to expect a similar sharp fall of Ω in the z-direction also, which is supported by the result for the experimental flame in figure 9. It is not possible to construct the two-point correlation function for the experimental flames along the z-direction using the single-shot PLIF images, and one needs imaging in all three dimensions with adequate resolution. However, from the visualization results presented in figure 12 of Chen *et al.* (2009) clearly showing the corrugations, contortions and foldings of the flame surface in three spatial dimensions, one can discern that the expected behaviour of Ω in three dimensions would be similar to that shown in figure 9. To conclude, note that the correlation length scale, defined below, is expected to be isotropic. Nevertheless, processing of Chen *et al.* (2009) data and more DNS and experimental data on the two-point correlation function would prove to be enlightening. The small oscillations observed in the correlation function for large values of Δ^{+} are due to the limited size of the sample available for averaging in the numerical flames, which has been verified by halving the sample size in this study as well as in an earlier study (Swaminathan *et al.* 2011).

The integral length scale normalised by the respective laminar flame thermal thickness, $\ell^{+} = \ell/\delta_L^o$, for the fluctuating reaction rate is calculated as

$$\ell^{+} = \int_{0}^{\infty} \Omega(\Delta^{+})\,\mathrm{d}\Delta^{+} \equiv F. \tag{4.2}$$

It is straightforward to see that $F = 0.5$ for the modelled correlation function given in (4.1). The values of F obtained directly from the DNS data for various simulations are shown in figure 10(a). Although the correlation function Ω becomes very small over a distance of about one to two δ_L^o, F varies in the range 0.1–0.65 from the leading side to the trailing side of the flame brush. A close study of this figure shows

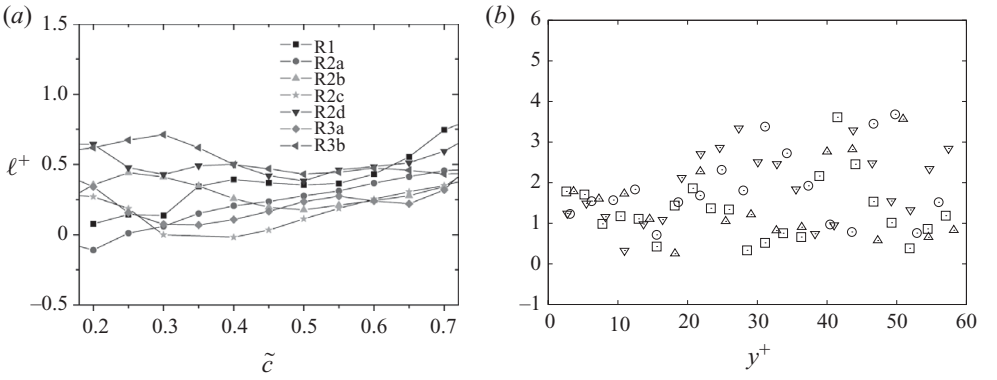

FIGURE 10. Typical variation of the normalised integral length scale, ℓ^+, for the reaction rate fluctuation in the DNS (*a*) and experimental (*b*) flames: ⊡, $\phi = 0.52$; ▽, 0.55; △, 0.58; ⊙, 0.64.

that this length scale takes a small negative value in one of the simulations (R2a), which is physically meaningless. This is because of the limited sample size and may also be taken to represent the accuracy of the numerics used in the data processing. Nevertheless, the normalised length scale obtained from the modelled correlation function seems acceptable.

The normalised integral length scale, ℓ^+, for few arbitrary locations in the experimental flames is shown in figure 10(*b*). These values are obtained by integrating numerical values of the corresponding two-point correlation function, Ω, as shown in figure 9. The negative value of Ω is observed to give $\ell^+ < 0.5$. Although the thickness of the averaged heat-releasing zone is larger than $10\delta_L^o$ in the downstream locations, the normalised integral length scale is found to be $\ell^+ \leqslant 4$. A reasonably good collapse of this normalised integral length scale for the different equivalence ratios considered in this study implies that it is predominantly controlled by the thermochemical process. These observations also hold even in swirling flames (Swaminathan *et al.* 2011). Furthermore, the statistical convergence is believed to be sufficient for the correlation statistics because of the short length scale associated with this correlation function.

Note that a quantity proportional to the heat release rate is obtained by multiplying the OH and CH_2O signals on the pixel-by-pixel basis as noted in § 3.2. This approach is markedly different from that of Wasle *et al.* (2005), who used a combination of OH-PLIF and chemiluminescence techniques. There, the flame front was identified using OH-PLIF and the chemiluminescence signals, representing the reaction rate integrated along the line of sight, gathered simultaneously from two photomultipliers were used to construct Ω. They deduced the correlation length scale for the fluctuating heat release rate to be of the order of local flame-brush thickness, which is nearly an order of magnitude larger than the correlation length scale obtained in this study, and this can lead to significant difference in the correlation volume required for (2.15).

4.3. *Correlation of the rate of change of the reaction rate fluctuation*

The two-point correlation for the time rate of change of the heat release rate fluctuation, Ω_1, is obtained using the procedure explained in § 2.2. This procedure requires the local velocities and progress variable gradients to evaluate $\partial c/\partial t$ using (2.11), which are not available for the experimental flames. Thus, the two-point correlation function Ω_1 is shown and discussed only for the numerical flames, and

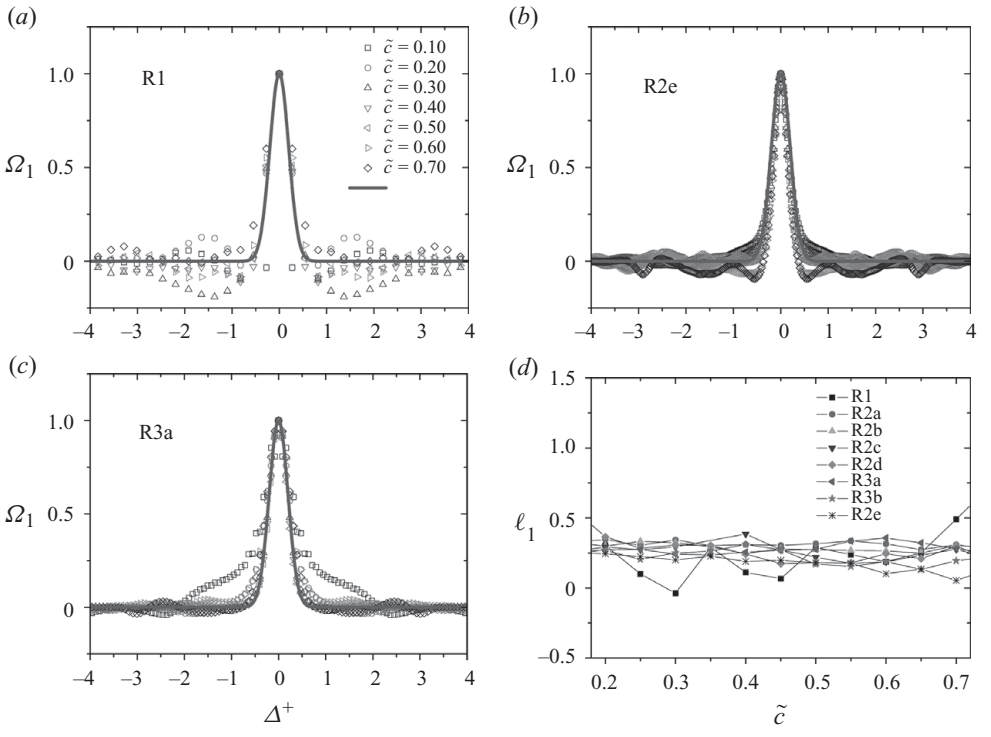

FIGURE 11. (*a–c*) Correlation function Ω_1 from three different simulations, R1, R2e and R3a. (*d*) The variation of the integral length scale ℓ_1^+ normalised using the respective δ_L^o across the flame brush is also shown for all eight simulations in table 1. The solid lines in (*a–c*) represent the model $\exp(-4\,\pi\Delta^{+2})$.

it is hoped that the observations made using these flames equally apply to the experimental flames also because of the similarities in the behaviour of Ω noted in § 4.2.

Typical variations of Ω_1 are shown in figure 11 for three different numerical flames at seven different locations inside the flame brush. The result for R2e from our preliminary study (Swaminathan *et al.* 2011) is also included here for completeness and to make the comparison easier. The correlation function is symmetric, similar to Ω, and drops from one to zero within about one thermal thickness. The oscillations of Ω_1 near zero are because of the limited sample size (Swaminathan *et al.* 2011). The sharp drop of Ω_1 with the separation distance implies that the integral length scale ℓ_1 is much smaller than ℓ. This is not surprising since $\ddot{\omega}$ involves the spatial gradients of c and the gradient of $\dot{\omega}$ in the progress variable space. The results in figure 11 are shown to indicate the influence of fuel type, stoichiometry and turbulence on the correlation function Ω_1. The turbulence Reynolds number for R1, R3a and R2e is respectively 57, 143 and 442. The flame R1 is a hydrocarbon-type flame while the other two flames are hydrogen–air flames with different stoichiometry. These results clearly suggest that the two-point correlation function Ω_1 is also insensitive to the fuel type and stoichiometry, turbulence and thermochemical conditions when the separation distance is normalised using the planar laminar flame thermal thickness. This behaviour is remarkable and simplifies considerably the problem of direct combustion noise as noted by (2.15).

An analytical curve of the form

$$\Omega_1(\Delta^+) = \exp(-4\pi\Delta^{+2}) \tag{4.3}$$

is also shown by a solid line for all three cases in figure 11 and this curve represents the data well. Some effects of numerical resolution are apparent for the simulation R1 (there are only three points for $|\Delta^+| \leqslant 0.5$). The integral length scale, ℓ_1, is obtained by integrating the calculated two-point correlation function and its value, normalised by the respective δ_L^o, is also shown in figure 11 for all of the eight numerical flames considered. Although this was shown in our earlier paper (Swaminathan *et al.* 2011), it is included here for comparison with figure 10(*a*). The collapse of the data is excellent across the flame brush and also for the various thermochemical and turbulence conditions considered for the DNS flames. A small negative value for the simulation R1 is because of numerical resolution. The normalised length scale, ℓ_1^+, obtained by integrating (4.3) is 0.25, which agrees very well with the data in figure 11. However, a direct measure of $\ddot{\omega}$ in DNS and experiments would be useful to put further confidence on this length scale.

An interesting point deduced from the above analysis is that the two-point correlation function, Ω_1, is strongly dictated by the thermochemical processes and thus the second integral in (2.15) is influenced by thermochemistry only. Thus, the expression for the far-field SPL given in (2.15) becomes

$$\overline{p'^2}(\boldsymbol{r}) = \frac{(\gamma-1)^2}{16\pi^2 r^2 a_o^4}\, Y_{f,u}^2\, H^2\, {\delta_L^o}^3 \int_{v_y} \frac{\mathscr{K}^2}{8}\, \overline{\dot{\omega}(y,t)}^2\, \mathrm{d}^3 y, \tag{4.4}$$

since the integration of Ω_1, in (4.3), over v_{cor} in spherical coordinates, gives ${\delta_L^o}^3/8$. The influence of turbulence on the combustion noise is felt via the remaining integral, over the flame-brush volume, since the mean reaction rate and v_y are controlled by the turbulence and its interaction with chemical reactions. Thus, one needs to obtain these two quantities, v_y and $\overline{\dot{\omega}}$, by direct computations rather than using semi-empirical correlations. Before addressing this, we study a possible modelling for $\mathscr{K}$.

4.4. *Modelling of* $\mathscr{K}$

As noted in § 2.2, the parameter $\mathscr{K}$ is given by $\mathscr{K} = \mathscr{B}_1\mathscr{B} = (\overline{\ddot{\omega}^2})^{1/2}/\overline{\dot{\omega}}$, where $\mathscr{B}_1$ is the inverse of an average time scale for the rate of change of the fluctuating heat release rate and $\mathscr{B}$ is the ratio of the fluctuating heat release rate to mean heat release rate. The values of $\mathscr{K}$ calculated directly from the DNS data and normalised using the respective laminar flame time are shown in figure 12 for five cases. There seems to be some variation of $\mathscr{K}^+$ across the flame brush; however; it remains almost constant in the middle of the flame brush and the sharp rise at the ends is due to the decrease in the mean reaction rate. The solid line denotes the arithmetic average of these five cases, which shows that $\mathscr{K}^+$ remains reasonably constant for major portion of the flame brush. In order to simplify the SPL calculation, discussed in the next section, it is taken that $\mathscr{K}^+ \approx 24$, and this value gives the inverse of the normalised time scale for the rate of change of the fluctuating reaction rate as $\mathscr{B}_1^+ \approx 33.95$ after using $\mathscr{B} \approx 0.707$ from figure 8. This value of $\mathscr{B}_1^+$ along with the experimentally determined value of $\mathscr{B}$ is used in (4.4) to obtain the SPL. Note also that the estimation of $\mathscr{K}^+$ needs further studies because of the approximations used to obtain $\ddot{\omega}$ and the size of the statistical samples. Thus, its values used here should be seen as tentative.

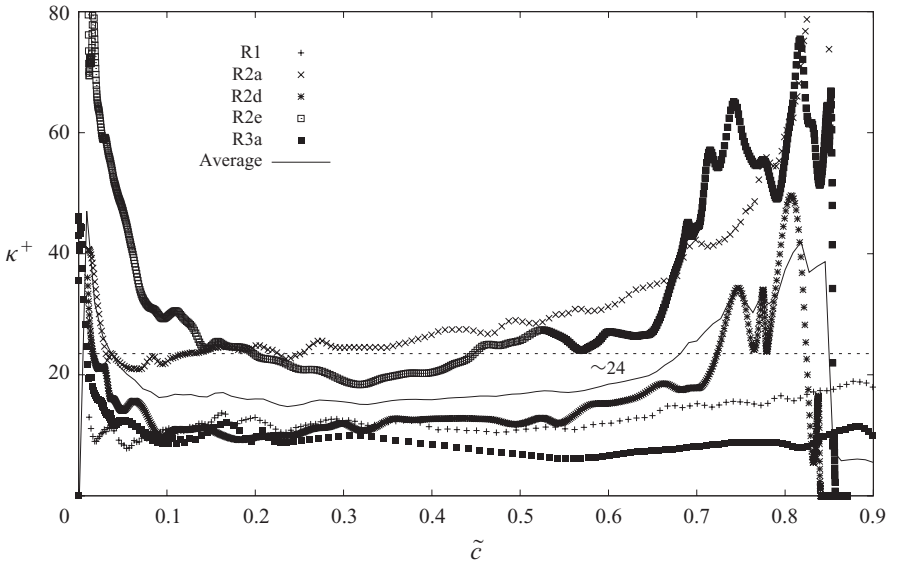

FIGURE 12. Typical variation of $\mathscr{K}^+$ across the flame brush.

5. Calculation of combustion noise level

Recently, sound emitted from statistically stationary, pilot-stabilised, turbulent premixed flames is reported by Rajaram (2007) and Rajaram & Lieuwen (2009) by measuring the far-field SPL. This experimental study considered a set of axisymmetric, with diameter D, turbulent jet premixed flames. These flames are marked as IDs in figure 2 and experience a wide range of turbulence and thermochemical conditions. The conditions of turbulence at the burner exit reported by Rajaram (2007) are used as boundary conditions in the calculations performed here. The turbulence intensity (u_{rms}/U_b) at the burner exit varies from about 0.8 % to 12.5 % and lean to stoichiometric conditions of acetylene–, natural gas– and propane–air mixtures are considered. The bulk mean velocity at the burner exit is denoted by U_b. Of a number of flame conditions reported by Rajaram (2007), 13 flames of natural gas– and propane–air mixtures are chosen arbitrarily. The conditions of these flames are given in table 2 and their combustion conditions are indicated in figure 2. The natural gas flames were considered in an earlier study (Swaminathan *et al.* 2011).

The acoustic measurements are made in an anechoic facility to eliminate the influence of reflected sound waves. The microphones for the acoustic measurements are located at $r = 1.02$ m and the maximum error in the measured SPL is estimated (Rajaram 2007) to be about ± 2 dB. Further details of these flames, measurement techniques and error estimates can be found in Rajaram (2007).

These flames are computed using steady RANS approach employing a standard $\widetilde{k}$–$\widetilde{\varepsilon}$ turbulence modelling with gradient flux approximations. In addition to the transport equations for the Favre- (density-weighted) averaged turbulent kinetic energy, $\widetilde{k}$, and its dissipation rate, $\widetilde{\varepsilon}$, other equations solved are for the conservation of the Favre-averaged mass, momentum and energy along with a balance equation for the Favre-averaged progress variable $\widetilde{c}$. This balance equation can be obtained by averaging (2.11), which requires a closure for the mean reaction rate, $\overline{\dot{\omega}}$. The density is obtained from the equation of state using the computed mean temperature. This is a standard practice in turbulent reacting flow calculations and the computations are carried out

No.	D (mm)	U_b (m s^{-1})	Fuel	ϕ	$\frac{u_{rms}}{U_b}$ (%)	$\frac{u_{rms}}{s_l^o}$	Q (kW)	SPL (dB)
ID1	10.9	21.8	NG	1.02	3.3	1.8	7.04	75
ID2	10.9	19	NG	0.82	2.8	1.77	4.99	67
ID3	10.9	21.8	NG	1.02	2.4	1.31	7.04	73
ID4	6.4	24.1	NG	0.9	0.8	0.54	2.38	67
ID5	6.4	24.1	NG	1.08	0.8	0.48	2.83	70
ID6	17.3	17.4	NG	1.02	4	1.74	14.16	76
ID7	34.8	8.6	NG	1.02	12.5	2.69	28.31	78
ID8	10.9	21.8	NG	0.95	1.5	0.81	6.59	75
ID9	10.9	16.3	Propane	0.67	2.2	1.84	3.35	63
ID10	6.4	32.2	Propane	0.8	0.7	0.74	2.71	70
ID11	17.3	17.4	Propane	1.03	11.5	4.67	13.55	83
ID12	17.3	17.4	Propane	1.03	2.4	0.97	13.55	78
ID13	17.3	8.7	Propane	0.99	4.1	0.83	6.54	71

TABLE 2. Experimental flames, marked as IDs in figure 2, used for the SPL calculation. Measured SPL in dB is also given.

using a commercially available computational fluid dynamics (CFD) tool along with a closure model for the mean reaction rate, $\overline{\dot{\omega}}$. The computational domain extends to $50D$ in the axial and $\pm 5D$ in the radial directions and axisymmetric calculations are performed because of the nature of these flames. A structured grid with a cell size of about 0.25 mm in the radial direction near the burner exit is used to capture the shear layer and the thin flame brush. This grid grows smoothly in the radial and axial directions and the results reported here are verified for grid dependency by doubling the smallest cell size. The mean reaction rates obtained from these calculations along with the results on the two-point correlation functions discussed above are then used in (2.15) to obtain the SPL.

5.1. *Mean reaction rate closure*

The mean reaction rate is obtained using a simple and fundamentally sound closure derived from the first principles by Bray (1979) for high Damköhler number premixed combustion, which is the case for the experimental flames considered here (see figure 2). This closure is written as

$$\overline{\dot{\omega}} \approx \frac{2}{(2C_m - 1)} \overline{\rho}\, \widetilde{\epsilon}_c, \tag{5.1}$$

where $C_m \equiv \overline{c\,\dot{\omega}}/\overline{\dot{\omega}}$ is a model parameter, which is known (Bray 1980) to be about 0.7 for hydrocarbon flames. The symbol $\widetilde{\epsilon}_c$ is the Favre mean scalar dissipation rate defined as $\overline{\rho}\,\widetilde{\epsilon}_c \equiv \overline{\rho\alpha(\nabla c'' \cdot \nabla c'')}$, where c'' is the Favre fluctuation of the progress variable and α is the diffusivity of c. This quantity denotes one-half of the dissipation rate of the Favre variance of c. The above closure is related to the eddy dissipation ideas of Spalding (1971), which are based on an analogy of the Kolmogorov energy cascade hypothesis. Physically, this model implies that the mean reaction rate is proportional to the average rate at which hot products and cold reactants are brought together by turbulence. Recent studies (Kolla *et al.* 2009, 2010) have shown that the above model is very good provided the scalar dissipation rate closure includes the effects of turbulence, heat release, molecular diffusion and their interactions with one another. Such a closure for the scalar dissipation rate is developed recently (Swaminathan & Grout 2006; Chakraborty, Rogerson & Swaminathan 2008; Kolla

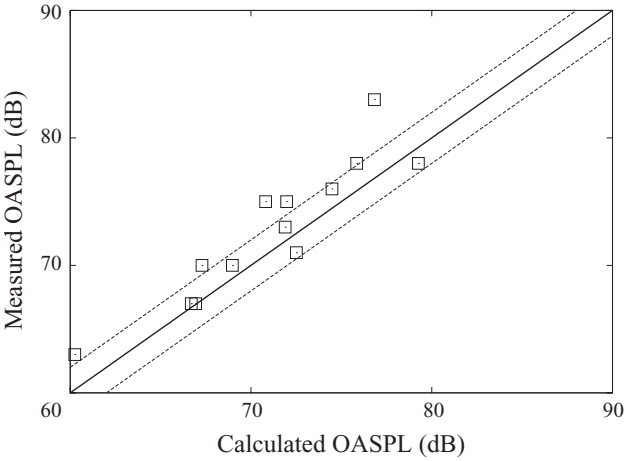

FIGURE 13. Comparison of the calculated and measured (Rajaram 2007) SPL. The dashed lines indicate ± 2 dB in the measurements and the solid line with unit slope is drawn for comparison.

et al. 2009), which is written as

$$\widetilde{\epsilon}_c = \frac{1}{\beta'}\left[(2K_c^* - \tau C_4)\frac{s_L^o}{\delta_L^o} + C_3\frac{\widetilde{\varepsilon}}{\widetilde{k}}\right]\widetilde{c''^2}, \tag{5.2}$$

where τ is the heat release parameter defined earlier. The model parameters in (5.2) are closely related to the physics of the reactive scalar mixing and thus their values cannot be changed arbitrarily. The values of these parameters are $\beta' = 6.7$, $K_c^* = 0.85\tau$ (for hydrocarbon–air mixtures); $C_3 = 1.5\sqrt{Ka}/(1+\sqrt{Ka})$ and $C_4 = 1.1/(1+Ka)^{0.4}$, where Ka is the Karlovitz number defined as $Ka^2 \equiv [2(1+\tau)^{0.7}]^{-1}(u_{rms}/s_L^o)^3(\delta_L^o/\Lambda)$ with $u_{rms} = (2\widetilde{k}/3)^{1/2}$ and $\Lambda = u_{rms}^3/\widetilde{\varepsilon}$. Further details are discussed by Kolla *et al.* (2009). The mean reaction rate is closed using (5.1) and (5.2) and the Favre variance of the progress variable, $\widetilde{c''^2}$, is obtained using its transport equation in the computations. The chemical source term in the variance transport equation is closed consistently using $2\,\overline{\dot{\omega}''c''} = 2(C_m - \widetilde{c})\,\overline{\dot{\omega}}$.

5.2. *SPL calculation*

Results of the RANS calculations are post-processed to obtain $\overline{\dot{\omega}}^2(R,z)$ and typical variation of $\overline{\dot{\omega}}(R,z)$ is shown in figure 14, which will be discussed later. Since the turbulent flame is axisymmetric, the differential volume for the integration in (4.4) is $\mathrm{d}^3y = 2\pi R\,\mathrm{d}R\,\mathrm{d}z$ and the integral is evaluated over the flame brush denoted by the coloured region in figure 14 appropriately. The overall SPL calculated thus is shown in figure 13 for all of the 13 flames in table 2 and the error bars of ± 2 dB shown are from Rajaram (2007). The flames ID1–ID8 are natural gas–air flames considered in an earlier study (Swaminathan *et al.* 2011) and ID9–ID13 are propane–air flames. The comparison between the calculated and measured pressure levels is very good except for the flame ID11, for which there is an underprediction of about 8 dB. From table 2, one notices that this flame has the highest u_{rms}/s_l^o value, its heat load is the same as for the flame ID12 and also it is almost close to that for the flame ID6. Thus, the most likely cause for this underprediction may be the estimation of the time scale involved in $\mathscr{K}$. As noted in § 4.3, this time scale will be influenced by turbulence and its interaction with chemistry. Hence, one needs to have a rigorous modelling and

treating $\mathscr{B}_1$ to be a constant may not be so good for large turbulence levels. A direct measurement of this quantity in DNS and experiments would be very useful to shed more light on a possible modelling. Nevertheless, the level of agreement shown in figure 13 is noteworthy, given the simple forms of (4.4) and the algebraic models (5.1) and (5.2) used in the calculations. Note also that none of the model parameters are tuned to capture the variations noted in figure 13.

5.3. *Discussion*

The analysis of the cross-correlation of the heat release rate fluctuation and its temporal rate of change enabled us to identify the effects of thermochemistry, turbulence and their interactions on the far-field SPL. This has helped to simplify the calculation of the far-field SPL and to obtain the spatial distribution of the combustion noise source. This spatial information can be used to extract the effects of turbulence and its interaction with chemical reactions on the amount of sound emitted from different regions of the flame brush. Figure 14 shows the spatial variation of $\overline{\dot{\omega}}(R, z)$ in three different flames, ID11, ID12 and ID13. The mean reaction rate is normalised by the respective $\rho_u s_L^o/\delta_L^o$ and the distances are normalised by the burner exit diameter, D. These three flames are chosen to elucidate the effects of (i) heat load (by changing the bulk mean velocity, U_b) and (ii) the turbulence level, for a given fuel–air mixture, on the distribution of combustion noise source. The flames ID11 and ID12 have the same heat load but substantially different turbulence level, u_{rms}/s_l^o. The flame ID12 has nearly the same turbulence level of the flame ID13, but it has about twice the heat load of flame ID13. Since the mixture equivalence ratio of these three flames is nearly the same, the colour maps in figure 14 show that the level of $\overline{\dot{\omega}}$ is almost the same, except at the burner exit, in these three flames. However, the size of the flame brushes and thus their volumes are different. The flame brush is short and broad in ID11 because of the large u_{rms}/s_l^o as one would expect. The length of the computed flame brush, l_f, is about $3D$ for this flame. The flame brush is long (about $5.2D$) and thin in ID12 because of the low-turbulence level despite the same bulk mean velocity, burner diameter and thus the heat load as in ID11. Note also that there is a drop in the measured SPL by about 5 dB and the calculated value differs from the measured value by about 2 dB. A more extensive and uniform spatial distribution of $\overline{\dot{\omega}}$ is predicted to have a lower noise level, since the SPL is proportional to $\int \overline{\dot{\omega}}^2 \,\mathrm{d}^3 y$ for a given heat load, which is given by $\int \overline{\dot{\omega}} \,\mathrm{d}^3 y$. Although the direct influence of u_{rms} on the SPL and thus on the thermoacoustic efficiency noted here has been observed in the experiments of Kilham & Kirmani (1979) and Kotake & Takamoto (1990), it is not captured in many of the scaling laws for high-Damköhler-number flames proposed in earlier studies (see the Introduction). A decrease in the bulk mean velocity, thus in the heat load, has obvious effects in ID13; a short flame with a length of about $2.7D$ and a substantially reduced SPL. The measured value is about 71 dB and the calculated value is about 72 dB.

Another quantity of interest that can be extracted from figure 14 is as follows. By writing the volume integral in (4.4) for a combustion zone that is axisymmetric in the mean, one obtains

$$\int_{v_f} \overline{\dot{\omega}}^2 \mathrm{d}^3 y = l_f D^2 \int_0^1 \mathrm{d}\hat{z} \int_{\hat{R}_1}^{\hat{R}_2} 2\pi \hat{R}\, \overline{\dot{\omega}}^2(\hat{R}, \hat{z})\, \mathrm{d}\hat{R}$$
$$= \int_0^1 \mathscr{W}(\hat{z})\, \mathrm{d}\hat{z} = \mathscr{W}_{max}, \tag{5.3}$$

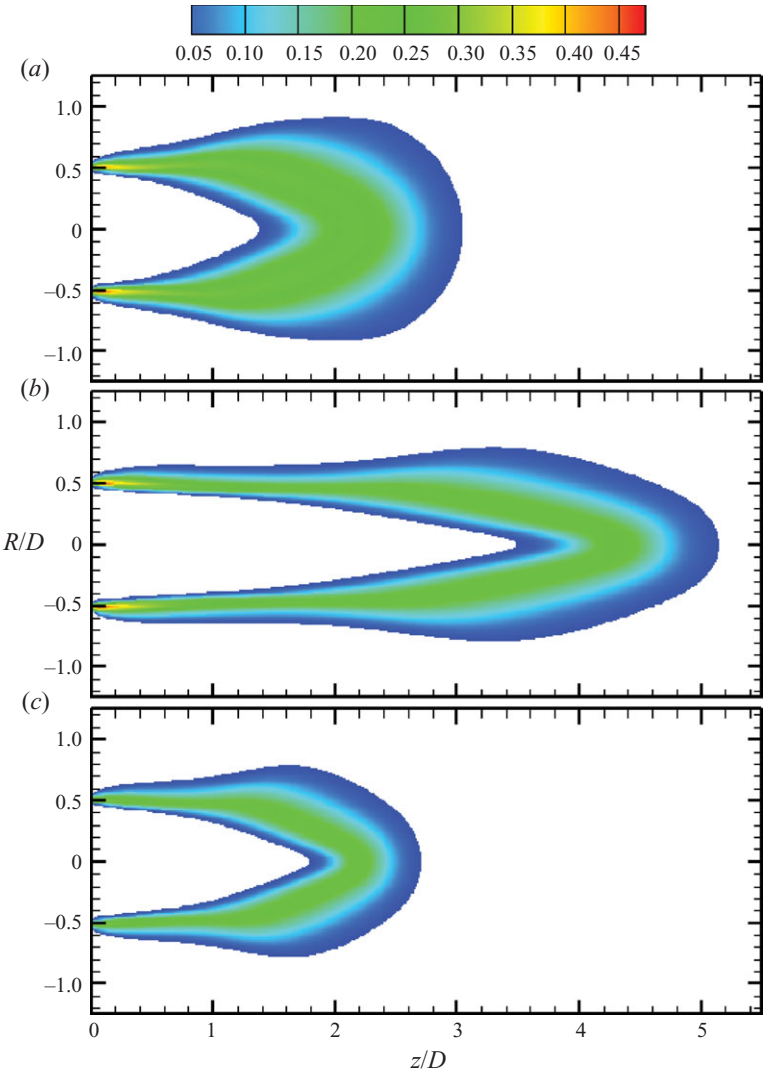

FIGURE 14. Colour map of the mean reaction rate $\overline{\dot{\omega}}$, normalised by $(\rho_u S_L^o/\delta_L^o)$, computed for the flames (*a*) ID11, (*b*) ID12 and (*c*) ID13.

where $\hat{R} = R/D$ and $\hat{z} = z/l_f$ and the limits $\hat{R}_1$ and $\hat{R}_2$ depend on $\hat{z}$ (see figure 14). The quantity $\mathscr{W}(\hat{z})/\mathscr{W}_{max}$ represents the fractional contribution from a given axial plane at distance $\hat{z}$ from the burner exit to the total sound pressure level in the far field. The variation of computed values of this ratio with $\hat{z}$ shown in figure 15 indicates a similar behaviour in the flames ID11 and ID13. This is because of the similarity in the flame-brush shapes shown in figure 14. For these flames, the maximum contribution comes from locations in the region $0.5 \leqslant \hat{z} \leqslant 0.65$. Although the reaction rate is very large near the burner exit, the integrated contribution from this region ($\hat{z} \leqslant 0.2$) is not large. However, for the flame ID12, with large heat load and low-turbulence level, there is a substantial contribution from this near-field region of the burner and the contribution per unit length of the flame brush reaches a minimum value at about

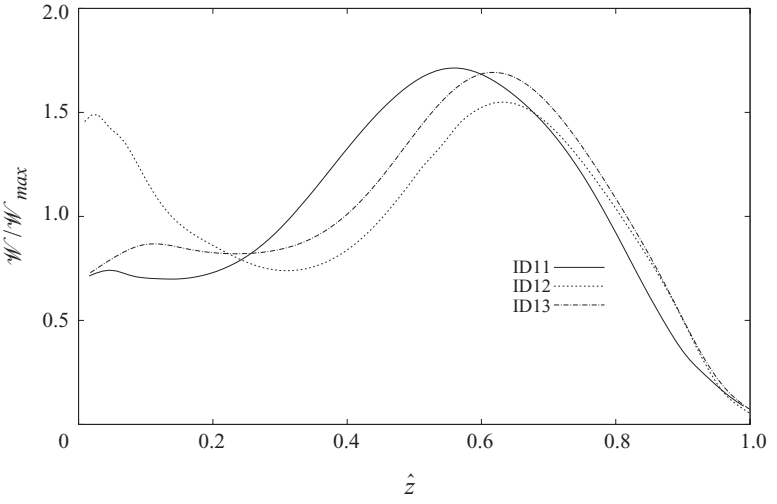

FIGURE 15. Variation of $\mathscr{W}(\hat{z})/\mathscr{W}_{max}$ with $\hat{z}$.

$\hat{z} = 0.3$. By studying figures 14 and 15 together, one observes that the subsequent increase in the value of $\mathscr{W}/\mathscr{W}_{max}$ is predominantly due to the increase in the annular area of the flame brush. This area increases first with downstream distance $\hat{z}$ and then decreases. A combined contribution of this area change with the mean reaction rate variation leads to the behaviour of $\mathscr{W}/\mathscr{W}_{max}$ shown in figure 15. Despite the differences in the conditions of these flames, a similar behaviour of $\mathscr{W}/\mathscr{W}_{max}$ after about $\hat{z} = 0.2$ is worth noting.

6. Conclusion

The two-point spatial correlation of the rate of change of the fluctuating heat release rate is central in combustion noise calculation. In this study, the heat release rate data from high-fidelity numerical simulations and advanced laser diagnostics is analysed to understand the behaviour of this two-point correlation in turbulent premixed flames. This understanding is then applied to predict the far-field SPL from open flames reported by Rajaram (2007). These three sets of turbulent flames cover a wide range of turbulent combustion conditions which are complementary to one another.

The numerical flames considered for the analysis covered a wide range of thermochemical and fluid dynamic conditions and include a hydrocarbon-like flame and hydrogen–air flames for a range of equivalence ratios. In addition, heat release rate information deduced from simultaneous planar laser-induced fluorescence of OH and CH_2O of axisymmetric bluff-body stabilised ethylene–air premixed turbulent flames for a range of equivalence ratios is used. The r.m.s. values of the fluctuating heat release rate normalised by its mean value are observed to be of order one because of the highly intermittent nature of the reaction rate signal.

The instantaneous rate of change of the fluctuating heat release rate is deduced using a balance equation for the fuel mass fraction-based progress variable and taking the instantaneous reaction rate to be a function of this progress variable and temperature. The two-point spatial correlation of the fluctuating heat release rate and the temporal rate of change of the fluctuating heat release rate constructed using these data clearly demonstrates that a Gaussian-type function can be used

to model these correlations and their integral length scales scale with the planar laminar flame thermal thickness. These integral length scales may, perhaps, be related to the length scale of flame wrinkling and further detailed analyses are required to assess this point. A comprehensive analysis of these correlation functions and their length scales using the experimental and numerical data suggests that (i) they are nearly isotropic and depend only on the separation distance Δ, (ii) fuel-type and its stoichiometry do not influence them and (iii) the Damkohler and turbulence Reynolds numbers have no effects on these quantities. These conclusions are then used to show explicitly that the influences of turbulence and thermochemistry on the far-field SPL, as in (2.15). The influence of turbulence is felt through the mean heat release rate while the thermochemical effects are felt through the cross-correlation function.

A detailed analysis of the rate of change of the fluctuating heat release rate suggests that the time scale for this quantity is about $\tau_c/34$, where τ_c is the planar laminar flame time scale (δ_L^o/S_L^o), on an average. A direct measurement of this quantity would be very useful, which is unavailable currently and further studies to address this time scale will be enlightening.

The open turbulent premixed flames of Rajaram (2007) are computed using standard $\widetilde{k}$–$\widetilde{\varepsilon}$ turbulence closure and an algebraic reaction rate model involving the dissipation rate of the progress variable variance (Bray 1979). The dissipation rate is obtained using a recently developed model (Kolla *et al.* 2010, 2009) which accounts for turbulence, chemical reactions, molecular diffusion and their strong interactions in premixed flames. The far-field SPL values calculated by post-processing the RANS results and using (4.4) agree well with the measured values and clearly suggest that this pressure level is low when the heat release rate is extensive and uniform spatially. Despite the very good agreement obtained for the SPL, it is noted that the frequency content of the emitted sound is not addressed in this work and will be considered in future as it requires two-point space–time correlation functions. Also, the sensitivity to combustion modelling is of some interest for further investigation.

The help of Dr Tanahashi and Shiwaku of the Tokyo Institute of Technology in transferring the DNS data via an EPSRC project is acknowledged. Dr Ayoola's help while acquiring PLIF images is acknowledged. G. Xu acknowledges the support from the National Natural Science Foundation of China by grants 50976116 and 50806077.

Appendix A. Derivation of (2.4)

Since the thermodynamic sources are in the term $\partial^2\rho_e/\partial t^2$ of (2.2), it has been shown in the following discussion how this term can be related directly to thermochemical and thermophysical processes. Detailed derivation can be found in Crighton *et al.* (1992). First, by substituting $\rho_e = (\rho - \rho_o) - (p - p_o)/a_0^2$ into the right-hand side of (2.3), one obtains

$$\frac{\partial \rho_e}{\partial t} = \frac{\rho_o}{\rho}\frac{\mathrm{D}\rho}{\mathrm{D}t} + \frac{(p-p_o)}{\rho\, a_o^2}\frac{\mathrm{D}\rho}{\mathrm{D}t} - \frac{1}{a_o^2}\frac{\mathrm{D}p}{\mathrm{D}t} - \frac{\partial\, u_i \rho_e}{\partial x_i}. \tag{A 1}$$

The energy conservation and thermodynamic relations are used to obtain $\mathrm{D}\rho/\mathrm{D}t$. The thermodynamic state relation for a multi-component mixture $p = p(\rho,\, s,\, Y_m)$,

where s is the specific entropy and Y_m is the mass fraction of species m, gives

$$\frac{\mathrm{D}\rho}{\mathrm{D}t} = \frac{1}{a^2}\frac{\mathrm{D}p}{\mathrm{D}t} - \frac{1}{a^2}\left(\frac{\partial p}{\partial s}\right)_{\rho,Y_m}\frac{\mathrm{D}s}{\mathrm{D}t} - \frac{1}{a^2}\sum_{m=1}^{N}\left(\frac{\partial p}{\partial Y_m}\right)_{\rho,s,Y_n}\frac{\mathrm{D}Y_m}{\mathrm{D}t}, \tag{A 2}$$

after noting $a^2 = (\partial p/\partial\rho)_{s,Y_m}$. Now the total derivative of s is obtained using the calorific state relation $e = e(s,\ \rho,\ Y_m)$ as

$$\rho\frac{\mathrm{D}e}{\mathrm{D}t} = \rho T\frac{\mathrm{D}s}{\mathrm{D}t} + \frac{p}{\rho}\frac{\mathrm{D}\rho}{\mathrm{D}t} + \rho\sum_{m=1}^{N}\frac{\mu_m}{W_m}\frac{\mathrm{D}Y_m}{\mathrm{D}t}, \tag{A 3}$$

when the following thermodynamic definitions for temperature, T, chemical potential, μ_m, of species m and pressure, p, given respectively as

$$\left(\frac{\partial e}{\partial s}\right)_{\rho,Y_m} = T, \quad \left(\frac{\partial e}{\partial Y_m}\right)_{s,\rho,Y_n} = \frac{\mu_m}{W_m}, \tag{A 4}$$

$$\left(\frac{\partial e}{\partial \rho}\right)_{s,Y_m} = \left(\frac{\partial e}{\partial v}\right)_{s,Y_m}\left(\frac{\partial v}{\partial \rho}\right)_{s,Y_m} = \frac{p}{\rho^2}, \tag{A 5}$$

are used, where W_m is the molecular weight of species m. The left-hand side of (A 3) is replaced by the conservation equation for internal energy (sensible + chemical), e. This conservation equation for a compressible flow of a multi-component reacting mixture is given by (Poinsot & Veynante 2001)

$$\rho\frac{\mathrm{D}e}{\mathrm{D}t} = -\frac{\partial q_i}{\partial x_i} - p\frac{\partial u_i}{\partial x_i} + \tau_{ij}\frac{\partial u_i}{\partial x_j} + \dot{\mathscr{Q}} + \rho\sum_{m=1}^{N} Y_m\, f_{m,i} V_{m,i}, \tag{A 6}$$

where the energy flux vector given by $q_i = -\lambda\partial T/\partial x_i + \rho\sum h_m Y_m V_{m,i}$ with λ being the thermal conductivity of the mixture, h_m is the enthalpy of species m and $V_{m,i}$ is the diffusion velocity in the direction i. The contributions of the external heat addition, $\dot{\mathscr{Q}}$, and the body forces, f_m, are usually negligible in turbulent combustion of interest here. An equation for $\mathrm{D}s/\mathrm{D}t$ can be obtained by substituting (A 6) into (A 3) as

$$\rho T\frac{\mathrm{D}s}{\mathrm{D}t} = -\frac{\partial q_i}{\partial x_i} + \tau_{ij}\frac{\partial u_i}{\partial x_j} - \rho\sum_{m=1}^{N}\frac{\mu_m}{W_m}\frac{\mathrm{D}Y_m}{\mathrm{D}t}, \tag{A 7}$$

after using the mass conservation and some simple rearrangements. Substituting (A 7) into (A 2) and using the following thermodynamic relations (Crighton *et al.* 1992)

$$\frac{1}{\rho T a^2}\left(\frac{\partial p}{\partial s}\right)_{\rho,Y_m} = \frac{\alpha_v}{c_p}, \tag{A 8}$$

$$\frac{1}{a^2}\left[\frac{\mu_m}{T W_m}\left(\frac{\partial p}{\partial s}\right)_{\rho,Y_m} - \left(\frac{\partial p}{\partial Y_m}\right)_{\rho,s,Y_n}\right] = \frac{\rho\alpha_v}{c_p}\left(\frac{\partial h}{\partial Y_m}\right)_{\rho,p,Y_n}, \tag{A 9}$$

where α_v is the coefficient of volumetric expansion and c_p is the specific heat at constant pressure, one obtains

$$\frac{\mathrm{D}\rho}{\mathrm{D}t} = \frac{1}{a^2}\frac{\mathrm{D}p}{\mathrm{D}t} + \frac{\alpha_v}{c_p}\left(\frac{\partial q_i}{\partial x_i} - \tau_{ij}\frac{\partial u_i}{\partial x_j}\right) + \frac{\alpha_v}{c_p}\sum_{m=1}^{N}\left(\frac{\partial h}{\partial Y_m}\right)_{\rho,p,Y_n}\rho\frac{\mathrm{D}Y_m}{\mathrm{D}t}. \tag{A 10}$$

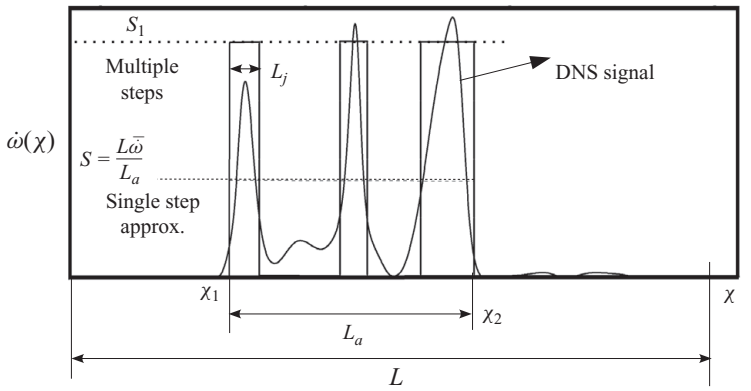

FIGURE 16. Typical reaction rate signal and its idealisation for analysis.

If the gases in the reacting multi-component mixture are taken to be ideal, then $(\partial h/\partial Y_m)_{\rho,p,Y_n}$ is the enthalpy of species m, h_m and $\alpha_v/c_p = (\gamma - 1)/a^2$. The ratio of specific heats is denoted by γ. The conservation of species m gives $\mathrm{D}Y_m/\mathrm{D}t = \dot{\omega}_m - \partial J_{m,i}/\partial x_i$, where $J_{m,i} = \rho V_{m,i} Y_m$ is the molecular diffusive flux of species m in the direction i. Using these relations in (A 10) and substituting the resulting expression in (2.3), one writes

$$\frac{\partial \rho_e}{\partial t} = -\frac{\partial u_i \rho_e}{\partial x_i} - \frac{1}{a_o^2}\left[\left(1 - \frac{\rho_o a_o^2}{\rho a^2}\right)\frac{\mathrm{D}p}{\mathrm{D}t} - \frac{p - p_o}{\rho}\frac{\mathrm{D}\rho}{\mathrm{D}t}\right] + \frac{\rho_o(\gamma - 1)}{\rho a^2}\left(-\dot{Q} + \frac{\partial q_i}{\partial x_i} - \tau_{ij}\frac{\partial u_i}{\partial x_j} - \sum_{m=1}^{N} h_m \frac{\partial J_{m,i}}{\partial x_i}\right), \quad \text{(A 11)}$$

where the heat release rate from chemical reactions is $\dot{Q} = -\sum_{m=1}^{N} h_m \dot{\omega}_m$. Now, it is straightforward to obtain (2.4) by substituting (A 11) into (2.2).

Appendix B. Relationship between mean and r.m.s. of intermittent signal-reaction rate

A typical reaction rate signal, taken from a randomly chosen position in the DNS, R2e, is shown in figure 16 and this sample signal can be idealised to be a telegraphic signal. Bray, Libby & Moss (1984) suggested this for progress variable c. These idealised signals are also shown in figure 16. The total length (here it is the size of the computational domain) of the signal is L and the reaction rate is non-zero in the interval $x_2 - x_1 = L_a$. If one approximates the reaction rate signal as a single pulse of size L_a and height S, then it can be shown that $S = L\bar{\omega}/L_a$ to keep the same average reaction rate, $\bar{\omega}$, given by the sample signal. One deduces that the r.m.s. of the reaction rate fluctuation normalised by the mean is

$$\left(\frac{\sqrt{\overline{\dot{\omega}'^2}}}{\bar{\dot{\omega}}}\right)_1 = \left(\frac{L}{L_a} - 1\right)^{1/2}, \quad \text{(B 1)}$$

after noting that

$$\overline{\dot{\omega}'^2} = \frac{1}{L}\int_0^L (\dot{\omega} - \bar{\dot{\omega}})^2 \, \mathrm{d}x. \quad \text{(B 2)}$$

The subscript 1 in (B 1) denotes that the reaction rate sample signal is approximated as a single pulse.

A typical intermittent signal will have a short length of intense activity followed by a relatively long lull period, as shown by the sample signal in figure 16, which has been idealised as three pulses. If one takes that the jth active pulse is of length L_j, then $S_1 = L\,\overline{\dot{\omega}}/\sum_j L_j$. Following the above procedure, one deduces that

$$\mathscr{B} \equiv \left(\frac{\sqrt{\overline{\dot{\omega}'^2}}}{\overline{\dot{\omega}}}\right)_n = \left(\frac{L}{\sum_{j=1}^{N} L_j} - 1\right)^{1/2}. \tag{B 3}$$

The active length, L_j, of the signal is expected to be smaller than the lull length in a highly intermittent signal. Thus, $\sum L_j \ll L$ and $\mathscr{B} > 1$. The above analysis equally applies to multi-dimensions as well as to time domain.

REFERENCES

Armitage, C. A., Balachandran, R., Mastorakos, E. & Cant, R. S. 2006 Investigation of the nonlinear response of turbulent premixed flames to imposed inlet velocity oscillations. *Combust. Flame* **146**, 419–436.

Ayoola, B. O., Balachandran, R., Frank, J. H., Mastorakos, E. & Kaminski, C. F. 2006 Spatially resolved heat release rate measurements in turbulent premixed flames. *Combust. Flame* **144**, 1–16.

Balachandran, R., Ayoola, B. O., Kaminski, C. F., Dowling, A. P. & Mastorakos, E. 2005 Experimental investigation of the nonlinear response of turbulent premixed flames to imposed inlet velocity oscillations. *Combust. Flame* **143**, 37–55.

Bilger, R. W. 1993 In *Turbulence and Molecular Processes in Combustion* (ed. T. Takeno), pp. 267–285. Elsevier.

Bragg, S. L. 1963 Combustion noise. *J. Inst. Fuel* **36**, 12–16.

Bray, K. N. C. 1979 The interaction between turbulence and combustion. *Proc. Combust. Inst.* **17**, 223–233.

Bray, K. N. C. 1980 Turbulent flows with premixed reactants. In *Turbulent Reacting Flows* (ed. P. A. Libby & F. A. Williams), pp. 115–183. Springer.

Bray, K. N. C., Libby, P. A. & Moss, J. B. 1984 Flamelet crossing frequencies and mean reaction rates in premixed turbulent combustion. *Combust. Sci. Tech.* **41**, 143–172.

Chakraborty, N., Rogerson, J. W. & Swaminathan, N. 2008 *A priori* assessment of closures for scalar dissipation rate transport in turbulent premixed flames using direct numerical simulation. *Phys. Fluids* **20**, 045106.

Chen, J. H., Choudhary, A., de Supinski, B., DeVries, M., Hawkes, E. R., Klasky, S., Liao, W. K., Ma, K. L., Mellor-Crummey, J., Podhorszki, N., Sankaran, R., Shende, S. & S.Yoo, C. 2009 Terascale direct numerical simulations of turbulent combustion using S3D. *Comput. Sci. Disc.* **2**, 015001, doi:10.1088/1749-4699/2/1/015001.

Clavin, P. & Siggia, E. D. 1991 Turbulent premixed flames and sound generation. *Combust. Sci. Tech.* **78**, 147–155.

Crighton, D. G., Dowling, A. P., Williams, J. E. F., Heckl, M. & Leppington, F. G. 1992 *Modern Methods in Analytical Acoustics: Lecture Notes*, chap. Thermoacoustic sources and instabilities, pp. 387–405. Springer.

Doak, P. E. 1972 Analysis of internally generated sound in continuous materials:2. a critical review of the conceptual adequacy and physical scope of existing theories of aerodynamic noise, with special reference to supersonic jet noise. *J. Sound Vib.* **25**, 263–335.

Dowling, A. P. 1976 Mean temperature and flow effects on combustion noise. *AIAA paper* 79-0590.

Duchaine, P., Zimmer, L. & Schuller, T. 2009 Experimental investigation of mechanism of sound production by partially premixed flames. *Proc. Combust. Inst.* **32**, 1027–1034.

Egolfopoulos, F. N., Zhu, D. L. & Law, C. K. 1990 Experimental and numerical determination of laminar flame speeds: mixtures of C_2-hydrocarbons with oxygen and nitrogen. *Proc. Combust. Inst.* **23**, 471–478.

Flemming, F., Sadiki, A. & Janicka, J. 2007 Investigation of combustion noise using a LES/CAA hybrid approach. *Proc. Combust. Inst.* **31**, 3189–3196.

Hartung, G., Hult, J., Kaminski, C. F., Rogerson, J. W. & Swaminathan, N. 2008 Effect of heat release on turbulence and scalar–turbulence interaction in premixed combustion. *Phys. Fluids* **20**, 035110.

Hassan, H. A. 1974 Scaling of combustion-generated noise. *J. Fluid Mech.* **66**, 445–453.

Hemchandra, S. & Lieuwen, T. 2010 Local consumption speed of turbulent premixed flames: an analysis of 'memory effects'. *Combust. Flame* **157**, 955–965.

Hirsch, C., Wasle, J., Winkler, A. & Sattelmayer, T. 2007 A spectral model for the sound pressure from turbulent premixed combustion. *Proc. Combust. Inst.* **31**, 1435–1441.

Hurle, I. R., Price, R. B., Sugden, T. M. & Thomas, A. 1968 Sound emission from open turbulent premixed flames. *Proc. R. Soc. Lond.* A **303**, 409–427.

Ihme, M., Pitsch, H. & Bodony, D. 2009 Radiation of noise in turbulent non-premixed flames. *Proc. Combust. Inst.* **32**, 1545–1553.

Jones, H. 1979 The generation of sound by flames. *Proc. R. Soc. Lond.* A **367**, 291–309.

Kilham, J. H. & Kirmani, N. 1979 The effect of turbulence on premixed flame noise. *Proc. Combust. Inst.* **17**, 327–336.

Klein, S. A. & Kok, J. B. W. 1999 Sound generation by turbulent nonpremixed flames. *Combust. Sci. Tech.* **149**, 267–295.

Kolla, H., Rogerson, J. W., Chakraborty, N. & Swaminathan, N. 2009 Scalar dissipation rate modelling and its validation. *Combust. Sci. Tech.* **181** (3), 518–535.

Kolla, H., Rogerson, J. W. & Swaminathan, N. 2010 Validation of a turbulent flame speed model across combustion regimes. *Combust. Sci. Tech.* **182**, 284–308.

Kotake, S. 1975 On combustion noise related to chemical reactions. *J. Sound Vib.* **42** (3), 399–410.

Kotake, S. & Takamoto, K. 1987 Combustion noise: effects of the shape and size of burner nozzle. *J. Sound Vib.* **112** (2), 345–354.

Kotake, S. & Takamoto, K. 1990 Combustion noise: effects of the velocity turbulence of unburned mixture. *J. Sound Vib.* **139** (1), 9–20.

Lighthill, M. J. 1952 On sound generated aerodynamically. I. General theory. *Proc. R. Soc. Lond.* A **211**, 564–587.

Lighthill, M. J. 1954 On sound generated aerodynamically. II. Turbulence as a source of sound. *Proc. R. Soc. Lond.* A **222**, 1–32.

Mahan, J. R. 1984 A critical review of noise production models for turbulent, gas-fueled burners. *Tech. Rep.* NASA CR–3803. NASA, Lewis Research Center.

Nada, Y., Shiwaku, N., Kikuta, S., Tannahashi, M. & Miyauchi, T. 2005 Fractal characteristics of hydrogen–air turbulent premixed flames. In *5th Asia-Pacific Conference on Combustion 2005*. The University of Adelaide, Australia.

Nada, Y., Tanahashi, M. & Miyauchi, T. 2004 Effect of turbulence characteristics on local flame structure of H_2–air premixed flames. *J. Turbul.* **5** (1), 1–15.

Najm, H. N., Knio, O. M., Paul, P. H. & Wyckoff, P. S. 1998 A study of flame observables in premixed methane–air flames. *Combust. Sci. Tech.* **140**, 369–403.

Ohiwa, N., Tanaka, K. & Yamaguchi, S. 1993 Noise characteristics of turbulent diffusion flames with coherent structure. *Combust. Sci. Tech.* **90**, 61–78.

Peters, N. 2000 *Turbulent Combustion*. Cambridge University Press.

Poinsot, T. & Veynante, D. 2001 *Theoretical and Numerical Combustion*. Edwards.

Price, R. B., Hurle, I. R. & Sugden, T. M. 1968 Optical studies of the generation of noise in turbulent flames. *Proc. Combust. Inst.* **12**, 1093–1101.

Rajaram, R. 2007 Characteristics of sound radiation from turbulent premixed flames. PhD thesis, Aerospace Engineering, Georgia Institute of Technology, Atlanta, Georgia, USA.

Rajaram, R. & Lieuwen, T. 2003 Parametric studies of acoustic radiation from premixed flames. *Combust. Sci. Tech.* **175**, 2269–2298.

Rajaram, R. & Lieuwen, T. 2009 Acoustic radiation from turbulent premixed flames. *J. Fluid Mech.* **637**, 357–385.

Rutland, C. J. & Cant, R. S. 1994 Turbulent transport in premixed flames. In *Proc. of Summer Program, Centre for Turbulence Research*, pp. 75–94. NASA Ames/Stanford University.

Singh, K. K., Frankel, S. H. & Gore, J. P. 2004 Study of spectral noise emissions from standard turbulent non-premixed flames. *AIAA J.* **42** (5), 931–936.

Singh, K. K., Zhang, C., Gore, J. P., Mongeau, L. & Frankel, S. H. 2005 An experimental study of partially premixed flame sound. *Proc. Combust. Inst.* **30**, 1707–1715.

Spalding, D. B. 1971 Mixing and chemical reaction in steady confined turbulent flames. *Symp. (Intl) Combust.* **13**, 649–657.

Strahle, W. C. 1971 On combustion generated noise. *J. Fluid Mech.* **49**, 399–414.

Strahle, W. C. 1973 Refraction, convection and diffusion flame effects in combustion generated noise. *Proc. Combust. Inst.* **14**, 527–535.

Strahle, W. C. 1976 Convergence of theory and experiment in direct combustion-generated noise. *Prog. Astronaut. Aeronaut.* **43**, 467–481.

Strahle, W. C. 1978 Combustion noise. *Prog. Energy Combust. Sci.* **4**, 157–176.

Strahle, W. C. & Shivashankara, B. N. 1975 A rational correlation of combustion noise results from open turbulent premixed flames. *Proc. Combust. Inst.* **15**, 1379–1385.

Swaminathan, N., Balachandran, R., Xu, G. & Dowling, A. P. 2011 On the correlation of heat release rate in turbulent premixed flames. *Proc. Combust. Inst.* **33**, 1533–1541.

Swaminathan, N. & Grout, R. W. 2006 Interaction of turbulence and scalar fields in premixed flames. *Phys. Fluids* **18**, 045102.

Wasle, J., Winkler, A. & Sattlemayer, T. 2005 Spatial coherence of the heat release fluctuations in turbulent jet and swirl flames. *Flow Turbul. Combust.* **75**, 29–50.